J. Indian Inst. Sci.
A Multidisciplinary Reviews Journal
ISSN: 0970-4140 Coden-JIISAD
© Indian Institute of Science 2017.

REVIEW ARTICLE

Multiscale Methods for Fracture: A Review★

P. R. Budarapu[1,2] and T. Rabczuk[3,4]*

Abstract | The global response of a system is often governed by the material behaviour at smaller length scales. Investigating the system mechanics at the smallest scale does not always provide the complete picture. Therefore, in the ambitious objective to derive the overall full-scale global response using a bottom-up approach, multiscale methods coupling disparate length and time scales have been evolved in the past two decades. The major objective of the multiscale methods is to reduce the computational costs by coupling the inexpensive coarse-scale/continuum based models with expensive fine-scale models. The fine-scale region is employed in the critical areas, such as crack tips or core of the dislocation. To improve the efficiency the fine-scale domain is adaptively adjusted as the defects propagate. As a result, the accuracy of the fine-scale model is combined with the efficiency of the coarse-scale model, arriving at a computationally efficient and accurate multiscale model. Currently, multiscale methods are applied to study problems in numerous fields, involving multiphysics. In this article, we present an overview of the multiscale methods for fracture applications. We discussed the techniques to model the coarse- and fine-scale domains, details of the coupling methods, adaptivity, and efficient coarse-graining techniques. The article is concluded with comments on recent trends and future scope.

Keywords: *Multiscale methods, Multiphysics, Computational fracture, Atomistic simulations, Coarse graining, Adaptivity*

1 Introduction

The global response of a system is often governed by the material behaviour at smaller length scales. For example, the macroscopic properties of a material such as toughness, strength, ductility, thermal and electrical conductivity, and chemical diffusion are strongly influenced by defects like cracks and dislocations, which are initiated and evolved at the nano scales. In the ambitious objective to derive the overall full-scale global response using a bottom-up approach, the sub-scale behaviour has to be accurately computed. Therefore, understanding the phenomena of material failure across multiple length scales has been the major research focus in the material science and engineering community for many years[1]. Although molecular dynamics (MD) simulations promise to reveal the fundamental mechanics of material failure at nano scales by modeling the atom-to-atom interactions, due to their small dimensions of the order of angstroms (Å), they are still prohibitively expensive to be employed in industrial applications[2,3]. A plausible alternative to reduce the computational demand is to couple the continuum scale with the discrete scale using a multiscale approach. In such paradigms, defects are explicitly modeled at the sub-scales, whilst a self-consistent continuum model elsewhere. Several numerical models dealing with multiple spatial and temporal length scales have been proposed in the past two decades[1,4–12]. Most of the coupling methods and simulations are focused on models of intact materials (without cracks). The transfer of information through different length scales

[1] *School of Mechanical Sciences, Indian Institute of Technology Bhubaneswar, Bhubaneswar 752050, India.* [2] *Department of Aerospace Engineering, Indian Institute of Science, Bangalore 560012, India.* [3] *Institute of Structural Mechanics, Bauhaus University of Weimar, 99423 Weimar, Germany.* [4] *Division of Computational Mechanics, Faculty of Civil Engineering, Ton Duc Thang University, Ho Chi Minh City, Vietnam.* ★ *Dedicated to the researchers of IISc.*
* *pattabhib@gmail.com*

Springer IISc Press

for problems involving material failure and finite temperatures still remains a challenging task. In this paper, an overview of the multiscale methods for fracture applications is presented. We denote the sub-scale domain the "fine scale region" and the continuum domain the "coarse scale region".

Multiscale methods are initiated through the quasi-continuum method (QCM)[1,13], by directly coupling the fine-scale region to the coarse-scale region. In the QCM, the continuum degrees of freedom need to be exactly located at the positions of the atoms at the interface, which is achieved by fine grading of the continuum mesh around the coupling region. The QCM has also been very successful at linking two continuum scales, for example, for fibrous materials[14] and is readily capable of including quantum effects through density functional theory (QCDFT)[15]. Beex et al.[16] have investigated four variants of the quasi-continuum method for their use in planar beam lattices which can also experience out-of plane deformation. Different frameworks are compared to the direct lattice computations for three truly multiscale test cases in which a single lattice defect is present in an otherwise perfectly regular beam lattice. The virtual-power-based quasi-continuum method is adopted for lattice models in which bond failure and subsequent frictional fiber sliding are incorporated, which are of significant importance for fibrous materials such as paper, cardboard, textile, and electronic textile[17]. Bond failure and fiber sliding are nonlocal dissipative mechanisms, which are treated with a mixed formulation in which the kinematic variables as well as the internal history variables are interpolated. Multiscale methods can be categorized into hierarchical[18–23], semi-concurrent[24–31] and concurrent methods[4,6–12,32–43], see Fig.1.

In hierarchical multiscale methods, see Fig. 1a, the information is passed from the fine-scale to the coarse-scale; but not vice versa. Computational homogenization[31,44–52] is a classical up-scaling technique. Hierarchical multiscale approaches are very efficient. Therefore, hierarchical methods have been successfully applied to study various problems, ranging from multiphase flow in porous media[53–55] to polymer nano-composites (PNC). An iterative multiscale finite volume method for the simulation of multiphase flow in fractured porous media in the context of a hierarchical fracture modeling framework is discussed in[18]. A hierarchical multiscale approach is employed in[21] to characterize the material behaviour of the heat-affected zone (HAZ) in welded connections. Liu et al.[56] developed a regularized phenomenological multiscale model, where the elastic properties are computed using direct homogenization and subsequently evolved using a simple three-parameter orthotropic continuum damage model. A unified regularization scheme was employed in the context of constitutive law rescaling and the staggered nonlocal approach. A hierarchical higher order multiscale cohesive zone model (MCZM) is introduced in[23], to simulate the fracture in crystalline solid, using up to third-order Cauchy–Born rules and Barycentric finite element method to construct shape functions for hexagonal shaped cohesive zones.

Lawrimore et al.[22] studied the mechanical responses of low volume fraction Polyvinyl Alcohol /Montmorillonite nano-composites using a hierarchical multiscale modeling method, by bridging the MD with finite element analysis (FEA). MD computations of interfaces were used to calibrate a traction–separation relation, which was then upscaled based on a cohesive zone model (CZM)[57–59]. Paggi et al.[20] estimated the influence of micro-cracking and power-loss in photovoltaic modules based on a global–local multi-physics multi-scale approach. The micro-scale damage mechanisms, particularly matrix/inter-phase fracture and fiber sliding in brittle ceramics, are studied in[60] based on multiscale methods. Nguyen et al.[50] have presented a computational homogenization procedure for cohesive and adhesive crack modeling of materials with a heterogeneous micro structure, for crack propagation under cyclic loading with numerical analysis of the convergence characteristics of the multiscale method and treatment of macroscopic snapback in a multiscale simulation. Greco et al.[61] have proposed a concurrent multiscale method to overcome the existing limitations on homogenization in the presence of strain localization in masonry structures. They adopted a multilevel domain decomposition approach equipped with an adaptive zooming-in criterion for detecting the zones affected by strain localizations.

However, hierarchical multiscale methods based on computational homogenization are not well suited to model fracture. One basic assumption of homogenization theories is the existence of disparate length scales[62]: $\mathcal{L}_{Cr} \ll \mathcal{L}_{RVE} \ll \mathcal{L}_{Spec}$, where $\mathcal{L}_{Cr}$, $\mathcal{L}_{RVE}$ and $\mathcal{L}_{Spec}$ are the size of the: crack, representative volume element (RVE) and specimen, respectively. The first condition is violated for problems involving fracture, as $\mathcal{L}_{Cr}$ is of the order of $\mathcal{L}_{RVE}$. Furthermore, periodic boundary conditions (PBC), often specified at the fine-scale, cannot be used when a crack touches a boundary as the displacement jump

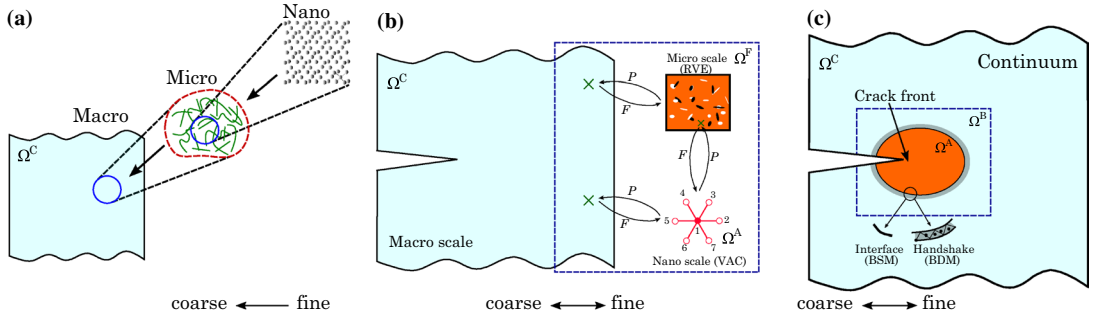

Figure 1: Schematics of **a** hierarchical, **b** semi-concurrent, and **c** concurrent multiscale methods. In the hierarchical methods the information exchange happens only from fine scale to coarse scale, whereas the interaction is two way in case of semi-concurrent and concurrent multiscale methods. Note a definite region of coupling in the concurrent multiscale methods, which does not exist in the semi-concurrent multiscale methods.

in that boundary violates the periodic boundary conditions.

Figure 1b illustrates the basic idea of semi-concurrent multiscale methods, where the information is passed from the fine-scale to the coarse-scale and vice versa. A classical semi-concurrent multiscale method is the FE ^{2}[24–27] method, originally developed for intact materials and later extended to problems involving material failure[9,45,48,49,63]. Oliver et al.[64] discussed the computational strategies to affordably solve multiscale fracture problems using FE ^{2} approach. Computational efficiency of the semi-concurrent multiscale methods is similar to concurrent multiscale methods[65]. The key advantage of semi-concurrent multiscale methods over concurrent multiscale methods is their flexibility, i.e., their ability to couple two different software packages, for example, MD software to FE software[66]. Zhu et al.[30] introduced a nonlinear semi-concurrent multiscale method to model crack propagation evolving from micro-structure for non-linear material behaviour based on an asymptotic expansion homogenization combined with the semi-concurrent finite element approach. Modified periodic boundary conditions and spherical grains' generation procedure are devised for nonlinear material model with post-failure stage. A semiconcurrent multiscale computational homogenization method for the simulation of hydro-mechanical problem for quasi-brittle materials is proposed in[31], coupling MD-models with continuum models. Silani et al.[29] have developed a semi-concurrent multiscale method to estimate the pre-localized damage initiation and propagation in the fully exfoliated clay/epoxy nanocomposite, where the methodology has been implemented in the commercial finite element software package ABAQUS. A macro-micro model has been implemented in ANSYS software[67], to predict matrix cracking evolution in laminates under in-plane loading by treating the transverse cracks as separate discontinuities in the micro-model. Kerfriden et al.[68] discussed a technique to reduce the computational burden associated with the simulation of localized failure in global–local framework. Recently, Ojo et al.[69] have proposed a non-local adaptive discrete empirical interpolation method combined with modified hp-refinement for order reduction of molecular dynamics systems.

Numerous concurrent multiscale methods have been developed that can be classified into 'Interface' coupling methods and 'Handshake' coupling methods, see Fig. 1c. The coupling happens along an interface in case of interface coupling methods[32], whereas, a definite region of coupling exists for the handshake coupling methods[7]. Interface coupling methods are not efficient for dynamic applications, as avoiding spurious wave reflections at the 'artificial' interface is problematic. On the other hand, since the coarse region does not exist everywhere, adaptive adjustment of the fine-scale region as the defects propagate in the handshake method is cumbersome. Some of the concurrent multiscale methods have been extended to modeling fracture[12,39,70]. Talebi et al.[43] have developed a concurrent coupling scheme coupling molecular dynamics to extended finite element method through the bridging domain method, to model three-dimensional cracks and dislocations at the atomistic level. Budarpu et al.[70] have proposed a solid shell-based concurrently coupled three-dimensional adaptive multiscale method (3DAMM) to simulate complex crack growth patterns in thin-walled

structures. The material in the bulk is modeled using a hybrid solid shell formulation relying on the combined use of the enhanced assumed strain (EAS) and the assumed natural strain (ANS) methods[71–75]. The authors developed a computational framework in MATLAB by triggering Large-scale Atomic/Molecular Massively Parallel Simulator (LAMMPS)[76] through `system` command.

In this paper, we present a review of the recent trends in multiscale methods for fracture applications. The article is structured as follows: multiscale methods are introduced in Sect. 1. Various techniques to model fine- and coarse-scale domains are discussed in Sect. 2 and 3, respectively. Section 4 is dedicated to the techniques on coupling the coarse- and fine-scale domains of concurrently coupled multiscale methods. Crack nucleation/growth criteria and the techniques for adaptive adjustment of the fine-scale region are discussed Sect. 5. Computer implementation steps of a three-dimensional enhanced bridging scale method based concurrently coupled multiscale method, in the MATLAB frame work are presented in Sect. 6. The article is concluded in Sect. 7 with a discussion on perspective future developments of multiscale methods.

2 Fine-scale modeling

In this section, various techniques to closely analyze the mechanics of fracture, particularly around the crack tip at lower scales are summarized. Popular techniques include atomistic models, virtual atom cluster models and representative volume element approaches.

2.1 Atomistic models

The basic structure of solid materials at nano scales can be obtained by the periodic arrangement of the unit lattice. Atoms in the lattice structure are bonded together by the van der Waals forces of attraction. Atomistic models are particle-based techniques, where the mechanics are simulated based on the atom–atom interactions. Furthermore, material characteristics depend on the arrangement of atoms in the crystal lattice and the forces of interaction such as mechanical, electrical, chemical, and thermal forces. Therefore, various types of potential functions are required to model the atom–atom interactions of various materials.

Consider a material such as Silicon used in the photovoltaic (PV) applications. Atoms in the Silicon unit cell are arranged in the diamond cubic lattice structure, where each Silicon atom possesses four nearest neighbors. Therefore, two Silicon atoms share four outer most atoms to form covalent bonds. When the Sun light equal to or more than a photon is incident on a PV cell, electrons from the outermost orbit are excited and released from their regular orbits, creating holes and free electrons. The free electrons are free to move throughout the crystal[77]. A photovoltage is generated by creating a potential barrier across the moving charges. On the other hand, micro-cracks in Silicon cells can lead to power losses up to 21%[78–82]. Therefore, the mechanics of a PV cell involves mechanical, thermal and electrical fields, requiring multiphysics-based techniques for accurate analysis[20,83–85]. Furthermore, MD simulations of multiphysics models demand potential functions such as charge optimized many body (COMB) potential[86], considering the combined effect of various fields.

The total potential energy ($E^{\text{tot}}(\text{q}, \mathbf{r})$), considering the effects of charge transfer, is expressed in terms of the electrostatic energies ($E^{\text{es}}(\text{q}, \mathbf{r})$), short-range interactions ($E^{\text{short}}(\text{q}, \mathbf{r})$), van der Waals interactions ($E^{\text{vdW}}(\mathbf{r})$), and correction terms ($E^{\text{corr}}(\mathbf{r})$), where $\mathbf{q}$ and $\mathbf{r}$ represent the charges and atom positions, respectively[86]:

$$E^{\text{tot}}(\mathbf{q},\mathbf{r}) = E^{\text{es}}(\mathbf{q},\mathbf{r}) + E^{\text{short}}(\mathbf{q},\mathbf{r}) + E^{vdW}(\mathbf{r}) + E^{\text{corr}}(\mathbf{r}). \quad (1)$$

The application of digital filters to split the energy spectrum of an atomistic zone simulated with molecular dynamics into low- and high-energy components is discussed in[87]. The effect of the grain orientation on the fracture behavior of polycrystalline silicon in micro-electro-mechanical systems has been investigated in[88], based on a multiscale model combining the discontinuous Galerkin method and extrinsic cohesive law describing the fracture process.

Techniques to simulate the fracture using atomistic models under static and dynamic scenarios are summarized in this section. Static conditions are achieved by minimizing the system potential energy, whereas velocity Verlet scheme[89] is a popular technique to estimate the atom velocities and positions.

2.1.1 Molecular dynamics

In molecular dynamics, the objective is to determine the atom positions $\mathbf{r}_\alpha(t)$, velocities $\mathbf{v}_\alpha(t)$, and their accelerations $\mathbf{a}_\alpha(t)$, for the given initial conditions. Each atom is assumed to be a classical particle obeying Newton's laws of mechanics. The

governing equations are derived from the Lagrangian equations mentioned below:

$$\frac{d}{\mathrm{d}t}\frac{\partial L}{\partial \dot{\mathbf{r}}_\alpha} - \frac{\partial L}{\partial \mathbf{r}_\alpha} = 0, \quad \alpha = 1, 2, 3, \ldots, n^{\mathrm{A}}, \tag{2}$$

where n^{A} represents the total number of atoms. The Lagrangian of the fine-scale domain can be estimated as follows:

$$L = \sum_{\alpha=1}^{n^{\mathrm{A}}} \frac{m_\alpha \dot{\mathbf{r}}_\alpha^2}{2} + \sum_{\alpha=1}^{n^{\mathrm{A}}} \mathrm{U}_\alpha(\mathbf{r}), \tag{3}$$

where m_α is the mass of the atoms and $U_\alpha(\mathbf{r})$ is the potential energy of the fine scale, which can be estimated as sum of all the bond potentials:

$$U_\alpha = \sum_{\alpha=1}^{n^{\mathrm{A}}} \phi_\alpha = \sum_{\alpha=1}^{n^{\mathrm{A}}} \left[\frac{1}{2} \sum_{\beta \neq \alpha}^{n^{\mathrm{A}}} V(r_{\alpha\beta}) \right], \tag{4}$$

where ϕ_α is the potential energy associated with atom α and β's denote all the neighbors of atom α. Therefore, substituting Eq. (3) in Eq. (2) yields the equations of motion in Newtonian form:

$$m_\alpha \ddot{\mathbf{r}}_\alpha = \frac{\partial \mathrm{U}(\mathbf{r}_\alpha)}{\partial \mathbf{r}_\alpha} = \mathbf{F}_\alpha, \quad \alpha = 1, 2, 3, \ldots, n^{\mathrm{A}}, \tag{5}$$

where $\mathbf{F}_\alpha$ is the internal force vector acting on atom α. Considering the initial conditions, Eq. (5) is solved for the trajectories of the atomic motion in the current configuration. Brief Verlet algorithm steps include the following: (1) solve Eq. (6) for the current atom positions

$$\mathbf{r}_\alpha(t + \Delta t) = \mathbf{r}_\alpha(t) + \mathbf{v}_\alpha(t)\Delta t + \frac{1}{2}\mathbf{a}_\alpha(t)\Delta t^2, \tag{6}$$

where (2) the atom velocites are estimated from

$$\mathbf{v}_\alpha(t + \Delta t) = \mathbf{v}_\alpha(t) + \frac{1}{2}[\mathbf{a}_\alpha(t) + \mathbf{a}_\alpha(t + \Delta t)]\Delta t, \tag{7}$$

in which (3) the accelerations in the current time step $\mathbf{a}_\alpha(t + \Delta t)$ in Eq. (7) are calculated from the interaction potential function and Eq. (5). Therefore, knowing the accelerations, atom velocities and positions can be estimated using Eqs. (7) and (6), respectively.

2.1.2 Molecular statics

In molecular statics (MS), the aim is to determine the positions of the atoms for the given boundary conditions, by minimizing the system potential energy, expressed as

$$\Pi = W^{\mathrm{int}} - W^{\mathrm{ext}}, \tag{8}$$

where W^{int} represents the internal energy of the system and W^{ext} is the external contribution. The system potential energy will be minimum when the first derivative of the potential function with respect to the positions of the atoms goes to zero. Therefore, the internal and external forces acting on an atom λ after the minimization of the potential energy are given by[12]:

$$\begin{aligned} \mathbf{F}_\lambda^{\mathrm{int}} &= \frac{1}{2}\sum_{\alpha=1}^{n^{\mathrm{A}}}\sum_{\beta\neq\lambda}^{n^{\mathrm{A}}} -\frac{\partial V(r_{\alpha\beta})}{\partial r_{\alpha\beta}}\frac{\partial r_{\alpha\beta}}{\partial \mathbf{r}_\lambda} \\ &= -\sum_{\beta\neq\alpha}^{n^{\mathrm{A}}} \frac{\partial V(r_{\alpha\beta})}{\partial r_{\alpha\beta}}\left(\frac{\mathbf{r}_\alpha - \mathbf{r}_\beta}{r_{\alpha\beta}}\right) \quad \text{and} \end{aligned} \tag{9a}$$

$$\mathbf{F}_\lambda^{\mathrm{ext}} = -\frac{\partial W^{\mathrm{ext}}}{\partial \mathbf{r}_\lambda}, \tag{9b}$$

respectively. The residual forces on each atom are estimated as $\mathbf{R} = \mathbf{F}^{\mathrm{int}} - \mathbf{F}^{\mathrm{ext}}$. Details of derivation of Eq. (9) and the computer implementation steps are explained in.[12]

Molecular dynamics simulations became important tools to understand the key mechanisms in wide range of applications. Therefore, over the years MD simulations attracted researchers in several fields, starting from early simulations of Abraham et. al.[2,90] for engineering applications to modern applications such as estimating the material properties[91–99], simulate problems involving multiphysics[20,100–105], model the mechanics of polymer nano composites[22,106–109] and bio-medical applications[110–114], to name a few. Therefore, several exclusive softwares have been evolved in the recent years to carry out MD simulations in various fields. Some of the popular softwares include (1) the open source Large-scale Atomic/Molecular Massively Parallel Simulator (LAMMPS)[76], with included potential functions to simulate the mechancis of soft and solid-state materials and coarse-grained systems. (2) Accelerated molecular dynamics simulations (ACEMD)[115,116]: an open source software to perform molecular dynamics simulations of proteins, oligosaccharides, nucleic acids, and synthetic polymers consisting of Chemistry at HARvard Macromolecular Mechanics (CHARMM), Amber forcefields and can run on NVIDIA graphics processing units (GPUs) optimized with CUDA. CUDA is a parallel computing platform and programming model that makes using a GPU for general purpose computing simple and elegant. (3) Abalone[117], a general purpose open source molecular modeling program focused on molecular dynamics of biopolymers, which can also interact with external quantum chemical programs ORCA, NWChem, CP2K, and PC GAMESS/Firefly. (4) GROningen

MOlecular Simulation (GROMOS)[110] is a software for dynamic modeling of bio-molecules. On the other hand, GROningen MAchine for Chemical Simulation (GROMACS)[118] is a parallel message-passing implementation of a MD program which is useful for bio(macro)molecules in aqueous environment. (5) AMBER[119] is a open source package of computer programs for applying molecular mechanics, normal mode analysis, molecular dynamics, and free energy calculations to simulate the structural and energetic properties of molecules. Apart from the above simulation softwares, there exist several supporting MD packages, for example, (1) PACKMOL[120] is a package for building initial configurations for molecular dynamics simulations and (2) Visual molecular dynamics (VMD)[121] is a popular visualization software to post process the MD simulation results.

2.2 Virtual atom cluster model

Virtual atom cluster (VAC) model is based on considering the symmetry of a crystal structure, where a cluster of atoms is taken as the representative model of the whole lattice structure[122,123]. As a result, all the calculations can be performed with reference to the representative cluster instead of the whole lattice, which leads to improved computational efficiency. Since the locations of atoms in the cluster do not represent the exact locations of the atoms, the representative cluster is called a virtual atom cluster (VAC). The same inter atomic potential as in the full-scale atomistic model can be used in the VAC model as well[12,122,124]. A full-scale atomistic model will be realized when the VAC assumes the structure of the underlying lattice. Therefore, VAC is an efficient coarse-graining technique to improve the computational efficiency.

A schematic of VAC-based coarse-scale model in two dimensions is shown in Fig. 2. The total potential energy of a fine-scale system as shown in Fig. 2a is given by the sum of all bond potentials ϕ_α, estimated using Eq. (4). Consider an equivalent coarse-scale model based on the VAC, illustrated in Fig. 2b. Since the fine-scale and coarse-scale models are equivalent, their potential energy must be equal. This is achieved by defining a distributed energy density function ϕ_ρ[122].

Considering the periodic nature of the lattice, ϕ_ρ is defined as the potential energy of a VAC divided by the volume of the VAC. For a homogeneous lattice, each VAC consists of a single atom and its volume is that of the unit cell of the lattice. Therefore, the distributed energy density function ϕ_ρ for a triangular lattice (see Fig. 2) can be defined as[12]:

$$\phi_\rho = \frac{\phi_{\mathrm{VAC}}}{V_0} = \frac{1}{2}\sum_{\beta=2}^{7}\frac{V(r_{1\beta})}{\sqrt{3}a^2/2} = \frac{1}{2}\sum_{\beta=2}^{7}\phi_{1\beta} \quad (10)$$

Therefore, using the definition of ϕ_ρ from Eq. (10), the internal nodal forces can be expressed as follows:[12]

$$\begin{aligned}\mathbf{F}_I^{\mathrm{int}} &\approx -\sum_{\mathrm{G}} w_{\mathrm{G}}\frac{\partial\phi_\rho^{\mathrm{G}}}{\partial\mathbf{u}}\frac{\partial\mathbf{u}}{\partial\mathbf{u}_I^{\mathrm{C}}}\\ &\approx -\sum_{\mathrm{G}} w_{\mathrm{G}}\sum_{\alpha=1}^{7}\frac{\partial\phi_\rho^{\mathrm{G}}}{\partial\mathbf{u}_\alpha^{\mathrm{C}}}\frac{\partial\mathbf{u}_\alpha^{\mathrm{C}}}{\partial\mathbf{u}_I^{\mathrm{C}}}\\ &= -\sum_{\mathrm{G}=1}^{n^{\mathrm{G}}} w_{\mathrm{G}}\sum_{\alpha=1}^{7}\frac{\partial\phi_\rho^{\mathrm{G}}}{\partial\mathbf{u}_\alpha^{\mathrm{C}}}N_I(\mathbf{X}_\alpha).\end{aligned} \quad (11)$$

The term $\frac{\partial\phi_\rho}{\partial\mathbf{u}_\alpha^{\mathrm{C}}}$ in Eq. (11) can be evaluated for each atom α in the VAC as given below:

$\alpha = 1$

$$\begin{aligned}\frac{\partial\phi_\rho}{\partial u_{1i}^{\mathrm{C}}} = &\frac{\partial\phi_{12}}{\partial r_{12}}\frac{r_{12i}}{r_{12}} + \frac{\partial\phi_{13}}{\partial r_{13}}\frac{r_{13i}}{r_{13}} + \frac{\partial\phi_{14}}{\partial r_{14}}\frac{r_{14i}}{r_{14}}\\ &+ \frac{\partial\phi_{15}}{\partial r_{15}}\frac{r_{15i}}{r_{15}} + \frac{\partial\phi_{16}}{\partial r_{16}}\frac{r_{16i}}{r_{16}} + \frac{\partial\phi_{17}}{\partial r_{17}}\frac{r_{17i}}{r_{17}}\end{aligned} \quad (12)$$

$\alpha = 2$–7

$$\frac{\partial\phi_\rho}{\partial u_{\alpha i}^{\mathrm{C}}} = -\frac{\partial\phi_{1\alpha}}{\partial r_{1\alpha}}\frac{r_{1\alpha i}}{r_{1\alpha}}, \quad (13)$$

where i is the index of the coordinate axes. The detailed derivation of the term $\frac{\partial\phi_\rho}{\partial\mathbf{u}_\alpha^{\mathrm{C}}}$ is given in appendix of[12]. Knowing the internal nodal forces in Eq. (11), the minimization problem can be solved for the coarse-scale solution by minimizing the potential energy for the given boundary conditions. An extension of the VAC-based coarse-graining scheme to study the dynamic fracture through a multiscale model is developed in.[124]

2.3 Representative volume element approach

Representative volume element approach is popularly used in the semi-concurrent multiscale methods (see Fig. 1b) to bridge the meso-scale to the macro-scale[29]. For fracture analysis based on the micro-mechanical approach using RVE, a damage parameter is estimated in meso-scale, which will be sent back to the macro-scale for further analysis. The boundary conditions for the RVE are extracted from the macro-scale model. Huang et al.[125] have analyzed the strain hardening

and multiple-cracking tensile fracture behavior of engineered cementitious composites, based on a multiscale method. The authors used a multilinear crack bridging relationship at a lower scale based on analytical crack bridging analysis for a single crack, whereas a representative volume element model was used at the upper scale using the extended finite element method. A global–local multiscale finite element method is employed in[126] to study the interaction of nanotubes and matrix at the nanoscale, based on building a 3D finite element model of a representative volume element around the crack tip. Paggi et al.[20] developed a multi-physics and multi-scale approach to study micro-cracking and power-loss in photovoltaic modules.

The size of the RVE depends on the dimension of the heterogeneities (d), which are expected to be much smaller than the dimension of the RVE. Therefore, the suitable size of the RVE for a particular problem can be arrived after few successive entanglement tests. For example, consider the ensemble average of the elastic modulus estimated based on different spatially random samples using different increasing RVE sizes, until the below stagnation condition is satisfied[29]:

$$\frac{|\langle E\rangle_{l'}^{(1)} - \langle E\rangle_{l}^{(1)}|}{\langle E\rangle_{l}^{(1)}} < \texttt{tol1}, \tag{14}$$

where $\langle E\rangle_{l}^{(1)}$ is the ensemble average for an RVE of size l, $\langle E\rangle_{l'}^{(1)}$ is the ensemble average for the RVE size of l', and `tol1` is a stagnation tolerance. A reasonable number of realizations for the estimation of the ensemble average can be estimated based on the below saturation criterion[29]:

$$\frac{|\langle E\rangle^{(2j)} - \langle E\rangle^{(j)}|}{\langle E\rangle^{(2j)}} < \texttt{tol2}, \tag{15}$$

where $\langle E\rangle^{(j)}$ denotes the ensemble average based on j realizations, $\langle E\rangle^{(2j)}$ indicates the ensemble average obtained using twice the number of realizations, and `tol2` is a saturation tolerance. The convergence can be guaranteed for 4 realizations with a convergence error of less than 1%.

3 Coarse-scale model

The coarse-scale domain might be discretized with classical techniques like the finite element method, the Partition of Unity Finite Element Method (PUFEM)[127,128], meshfree methods[6,129–132] or partition-of-unity enriched methods such as the extended Finite Element Method (XFEM)[133–141], the Smooth Finite Element Method (SFEM)[138,142–144], the Generalized Finite Element Method (GFEM)[145–150], the extended Element Free Galerkin method (XEFG)[151–158], the Cracking Particles Method[159–165], the Phantom node method (PNM)[166–172] or the Numerical Manifold Method (NMM)[173,174], the phase-field methods[102,175–178], Peridynamics[179,180], to name a few, apart from the isogeometric analysis with high-order approximation techniques[51,142,181–186] with exact geometry.

Alternative techniques to model fracture in shells include a FEM-based computational method for the fracture of plates and shells on the basis of edge rotation and load control as described in[187]. Rabczuk et al.[163] have developed a meshfree method for thin shells with finite strains and arbitrary evolving cracks, eliminating the membrane locking using a cubic or fourth-order polynomial basis. However, third-order complete formulations lead to the large support sizes, increasing the computational cost[188]. An extrinsic basis to increase the order of completeness of the approximation reduces the support size at

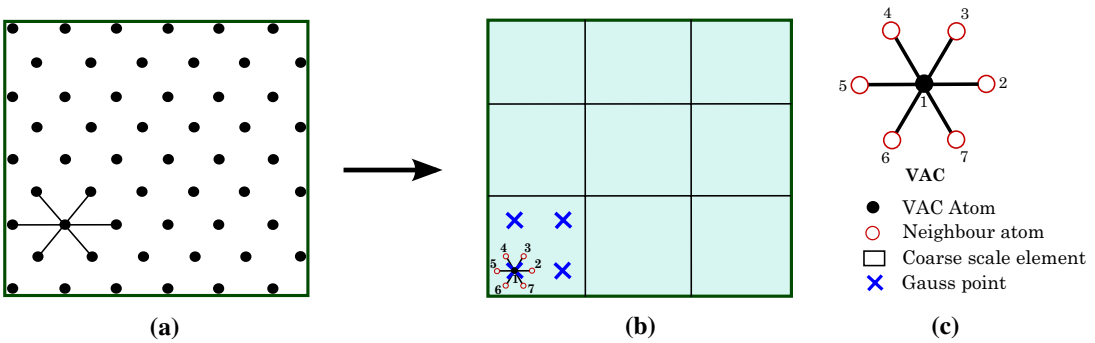

Figure 2: A demonstration of VAC coarse-scale model in two dimensions. **a** Atomistic model with triangular lattice as on the (111) plane of an fcc material. **b** Equivalent continuum model with the VAC being placed at a particular Gauss point. **c** Details of the VAC.

the cost of adding more degrees of freedom per node. Nonetheless, numerical experiments show a reduced CPU time for several problems. On the other hand, linear dependence of the shape functions deteriorates the conditioning of the final system of equations[188]. Reinoso et al.[74] devised and implemented a 7-parameter shell element for geometrically nonlinear analysis of layered CFRP composites. Nguyen et al.[189] proposed an extended isogeometric element formulation (XIGA) based on the Kirchhoff–Love theory, for the analysis of through-the-thickness cracks in thin shell structures based on Non-Uniform Rational B-Splines (NURBS).

Verhoosel et al.[63] employed a partition of unity-based cohesive zone finite element model to mimic crack nucleation and propagation in a piezoelectric continuum, through a multiscale framework to appropriately represent the influence of the microstructure on the response of a miniaturized component. Plews et al.[190] have proposed a generalized finite element approach for predicting localized, nonlinear, thermoplastic behavior and residual stresses and deformations in structures subjected to intense heating. A multiscale reduction technique to describe shale gas transport in fractured media is discussed in[191]. The matrix is described by upscaled models and the interaction between the matrix and the fractures is modeled through the generalized multiscale finite element method[192].

In this section, popular techniques to model cracks in the continuum, such as extended finite element method, meshless methods, phase field method and the phantom node method are discussed. Mathematical formulation of the last three methods are presented in detail.

3.1 Extended finite element method

Finite element methods, a powerful class of techniques to study a wide range of problems, fail to model the problems involving strong and weak discontinuities with a jump in the displacement and strain field, because of their smooth interpolation character. In other words, computational failure mechanics involving fracture related to the initiation and propagation of crack, which falls under the strong discontinuities, and interface problems involving interactions of solid–solid and fluid–fluid (weak discontinuities) and solid–fluid (strong discontinuities) are cumbersome to simulate using the FE techniques. Therefore, to handle linear and nonlinear crack openings, a very flexible extended finite element method has been developed by Belytschko et al.[193,194] based on the partition of unity concept[127,145] and through additional nodal parameters for the elements cut by the crack. The central idea of XFEM is to decompose the displacement field into a continuous part $\mathbf{u}^{\mathrm{C}}$ and a discontinuous part $\mathbf{u}^{\mathrm{D}}$:

$$\mathbf{u}(\mathbf{X}) = \mathbf{u}^{\mathrm{C}}(\mathbf{X}) + \mathbf{u}^{\mathrm{D}}(\mathbf{X}) \tag{16}$$

The discontinuous part ($\mathbf{u}^{\mathrm{D}}$) is estimated introducing the additional information into the FE interpolation through the local partition of unity approach by adding an enrichment, whereas the continuous part ($\mathbf{u}^{\mathrm{C}}$) is the standard FE interpolation. The approximation of the displacement field for n^{C} cracks with n^{T} crack tips reads

$$\begin{aligned}\mathbf{u}(\mathbf{X}) = &\sum_{I\in\mathcal{S}} N_I(\mathbf{X})\mathbf{u}_I + \sum_{K=1}^{n^{\mathrm{C}}}\sum_{I\in\mathcal{S}^{\mathrm{C}}} N_I(\mathbf{X})\psi_I^{\mathrm{K}}(\mathbf{X})\mathbf{a}_I^{\mathrm{K}} \\ &+ \sum_{M=1}^{n^{\mathrm{T}}}\sum_{I\in\mathcal{S}^{\mathrm{T}}} N_I(\mathbf{X})\sum_{P=1}^{N_{\mathrm{P}}}\phi_{PI}^{\mathrm{M}}(\mathbf{X})\mathbf{b}_{PI}^{\mathrm{M}},\end{aligned} \tag{17}$$

where $\mathcal{S}$ is the set of nodes in the entire discretization, $\mathcal{S}^{\mathrm{C}}$ is the set of nodes associated with completely cracked elements, $\mathcal{S}^{\mathrm{T}}$ is the set of nodes around the crack tip, N_I is the standard shape functions, $\psi_I^{\mathrm{K}}(\mathbf{X})$ is the enrichment function of Kth crack, ϕ_{PI}^{T} is the enrichment function for the crack tip P, $\mathbf{a}_I$, and $\mathbf{b}_{PI}$ are the additional degrees of freedom to be solved. Further details on XFEM and its applications can be found in the excellent review papers by Belytschko et al.[195], Fries and Belytschko[196], Karihaloo and Xiao[197], Rabczuk[66] or the book by Mohammadi[198].

3.2 Extended Meshless methods

Meshless methods (MM) evolved after the introduction of Element Free Galarkin (EFG) method by Belytschko[130]. They are based on the idea of using the nodes/particles in the zone of influence of a selected point to construct its approximation space. The particles are not connected; hence, it is particularly easy to simulate complex phenomena like fracture[129,157,161,165,199–202]. Popular meshless methods include Meshless Local Petrov-Galerkin (MLPG)[203,204], the reproducing kernel particle method (RKPM)[131,132], radial point interpolation method (RPIM)[205,206], to name a few. A meshless variational multiscale method for thermo-mechanical material failure is discussed in[101]. The displacement and temperature fields are enriched with step-functions and appropriate crack tip enrichment accounting for fine-scale features.

Yang et al.[207] have developed a meshless collocation method based on the differential reproducing kernel (DRK) approximation, where the

derivative of the shape function of reproducing kernel (RK) approximants is replaced by a set of differential reproducing conditions to avoid the complex direct differentiation. On the other hand, in the EFG[130,208] method, the shape functions are directly differentiated. Therefore, the number of degrees of freedom are reduced in DRK approximation, improving the computational efficiency of the DRKP method as compared to the RKPM. The Kronecker delta property is not satisfied by the shape functions of the RK approximants. To resolve the difficulty in the DRK approximation, a meshless collocation method based on the DRKP method has been introduced by ChingPing et al.[104,105,209,210], satisfying the Kronecker delta property.

Consider a body Ω in two-dimensional vector space $\mathcal{R}^2$ with boundary Γ, as shown in Fig. 3. The crack is denoted by c on the surface Γ_c.

3.3 Displacement field

A displacement field that is discontinuous at the crack(s) and continuous elsewhere in the domain Ω is a proper choice to model fracture in meshless methods. Therefore, the total displacement field is decomposed into a standard/continuous and discontinuous/enriched part:

$$\mathbf{u} = \mathbf{u}^{\text{cont}} + \mathbf{u}^{\text{enr}}, \tag{18}$$

where $\mathbf{u}^{\text{cont}}$ is the continuous component and $\mathbf{u}^{\text{enr}}$ is the discontinuous component. The meshfree approximation of Eq. (18) is given by

$$\mathbf{u}^{\text{h}}(\mathbf{X}) = \sum_{I\in\mathcal{S}} N_I^{\text{cont}}(\mathbf{X})\mathbf{u}_I + \sum_{I\in\mathcal{S}^{\text{c}}} N_I^{\text{enr}}(\mathbf{X})\mathbf{q}_I, \tag{19}$$

where N_I^{cont} and N_I^{enr} are the displacement interpolation/approximation functions in the continuous and discontinuous domains, respectively, see Fig. 4. $\mathbf{u}_I$ and $\mathbf{q}_I$ indicate the nodal parameters associated with the continuous and discontinuous displacement fields, respectively. The DRKP interpolant function $N_I^{\text{cont}}(\mathbf{X})$ is defined ask follows:

$$N_I^{\text{cont}}(\mathbf{X}) = \hat{N}_I(\mathbf{X}) + \bar{N}_I(\mathbf{X}), \tag{20}$$

where $\hat{N}(s)$ is estimated based on the quartic spline function. $\bar{N}_I(\mathbf{x})$ in Eq. (20), is introduced to impose the nth order reproducing conditions:

$$\bar{N}_I(\mathbf{X}) = w_a(\mathbf{X}-\mathbf{X}_I)\mathbf{P}^{\text{T}}(\mathbf{X}-\mathbf{X}_I)\bar{\mathbf{z}}(\mathbf{X}), \tag{21}$$

where the weight function $w_a(\mathbf{X}-\mathbf{X}_I)$ is centered at $\mathbf{X}_I$, defined by the normalized Gaussian function, and $\mathbf{P}^{\text{T}}(\mathbf{X}-\mathbf{X}_I)$ are the nth order polynomial functions. For an nth order complete polynomial basis, a set of reproducing conditions can be obtained to determine $\bar{\mathbf{z}}_i(\mathbf{X}), i = 1, 2, \ldots, n^{\text{B}}$, where n^{B} are the total number of basis functions given by $(n+1)(n+2)/2$. Further details of estimation of $\hat{N}_I(\mathbf{X})$ and $\bar{N}_I(\mathbf{X})$ functions are discussed in[42].

The enriched shape functions in Eq. (19) are expressed as the product of the standard shape function and the sign function $\mathcal{H}$:

$$N_I^{\text{enr}}(\mathbf{X}) = N_I^{\text{cont}}(\mathbf{X})\mathcal{H}(f_I(\mathbf{X})), \tag{22}$$

where

$$\mathcal{H}(\xi) = \begin{cases} 1 \forall \xi > 0 \\ -1 \forall \xi < 0, \end{cases} \tag{23}$$

and $f_I(\mathbf{X}) = \mathbf{n}_0 \cdot (\mathbf{X} - \mathbf{X_I})$, $\mathbf{n}_0$ is the normal of the split nodes in the initial configuration, estimated from the fine scale.

3.3.1 Variational formulation

The governing equations in weak form can be stated as follows: find $\mathbf{u} \in U, \forall \delta\mathbf{u} \in U_0$, such that,

$$\delta W = \delta W_{\text{int}} - \delta W_{\text{ext}} = 0, \tag{24}$$

where $\mathbf{u} = \bar{\mathbf{u}}$ on Γ_u and $\mathbf{u} \in \mathcal{H}(\Omega)$, δW_{int} is the first variation of the internal energy, and δW_{ext} is the virtual work from the external forces. Let the test functions $\delta\mathbf{u}^{\text{h}}(\mathbf{X})$ be defined as

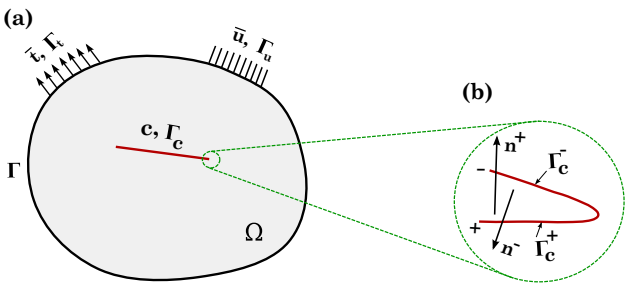

Figure 3: Domain and surface descriptions of a body **a** displacements, tractions and the crack along with their surfaces **b** a closeup of the crack tip indicating the directions on the normals on the crack surfaces.

$$\delta \mathbf{u}^{\mathrm{h}}(\mathbf{X}) = \sum_{I \in \mathcal{S}} N_I^{\mathrm{cont}}(\mathbf{X}) \delta \mathbf{u}_I + \sum_{I \in \mathcal{S}^c} N_I^{\mathrm{enr}}(\mathbf{X}) \delta \mathbf{q}_I. \tag{25}$$

Therefore, based on Eqs. (19), (24) and (25), the discrete system of equations can be obtained as[42]

$$\mathbf{K}_{IJ} \cdot \mathbf{d}_J = \mathbf{f}_I^{\mathrm{ext}}, \tag{26}$$

where $\mathbf{K}_{IJ}$ is the stiffness matrix, and $\mathbf{f}_I^{\mathrm{ext}}$ indicate the external force vector, and $\mathbf{d}_J$ is the vector containing the nodal parameters. The stiffness matrix is estimated as

$$\mathbf{K}_{IJ} = \int_{\Omega_0 \setminus \Gamma_0{}^c} \begin{bmatrix} \mathbf{K}_{IJ}^{uu} & \mathbf{K}_{IJ}^{uq} \\ \mathbf{K}_{IJ}^{qu} & \mathbf{K}_{IJ}^{qq} \end{bmatrix} \mathrm{d}\Omega, \tag{27}$$

where

$$\mathbf{K}_{IJ}^{uu} = \frac{\partial N_I^{\mathrm{cont}}(\mathbf{X})}{\partial \mathbf{X}} \mathbf{C} \frac{\partial N_J^{\mathrm{cont}}(\mathbf{X})}{\partial \mathbf{X}}, \tag{28a}$$

$$\mathbf{K}_{IJ}^{uq} = \frac{\partial N_I^{\mathrm{cont}}(\mathbf{X})}{\partial \mathbf{X}} \mathbf{C} \frac{\partial N_J^{\mathrm{cont}}(\mathbf{X}) \mathcal{H}(\mathbf{f}_J(\mathbf{X}))}{\partial \mathbf{X}}, \tag{28b}$$

$$\mathbf{K}_{IJ}^{qu} = \frac{\partial N_I^{\mathrm{cont}}(\mathbf{X}) \mathcal{H}(\mathbf{f}_I(\mathbf{X}))}{\partial \mathbf{X}} \mathbf{C} \frac{\partial N_J^{\mathrm{cont}}(\mathbf{X})}{\partial \mathbf{X}}, \tag{28c}$$

$$\mathbf{K}_{IJ}^{qq} = \frac{\partial N_I^{\mathrm{cont}}(\mathbf{X}) \mathcal{H}(\mathbf{f}_I(\mathbf{X}))}{\partial \mathbf{X}} \mathbf{C} \frac{\partial N_J^{\mathrm{cont}}(\mathbf{X}) \mathcal{H}(\mathbf{f}_J(\mathbf{X}))}{\partial \mathbf{X}}, \tag{28d}$$

where $\mathbf{C}$ is the matrix of material constants. The expressions for the nodal forces are given by[159]:

$$\mathbf{f}_I^{\mathrm{ext}} = \int_{\Omega_0 \setminus \Gamma_0^{\mathrm{c}}} N_I^{\mathrm{cont}}(\mathbf{X})^{\mathbf{T}} \mathbf{b} \mathrm{d}\Omega + \int_{\Omega_0 \setminus \Gamma_0^{\mathrm{c}}} N_J^{\mathrm{enr}}(\mathbf{X})^{\mathbf{T}} \mathbf{b} \mathrm{d}\Omega. \tag{29}$$

3.4 Phase-field method for fracture

Phase field (PF) approaches have been extensively used over the years for several different engineering applications[175,176,211–213]. The PF approach has been proven to be very effective and accurate to simulate complex fracture patterns[177,178,214–216], even at nano-scales[217]. On the other hand, PF model requires very fine discretizations to accurately capture failure in solids, which is computationally expensive. Based on the value of the phase field parameter ($\mathfrak{d}$), the orientation of the crack surface and the approximate location of the crack tip can be identified. Giovanardi et al.[218] proposed a global–local approach by coupling XFEM in the caorse scale with the phase field model at the fine scale. Yingjun et al.[217] developed a multiscale method based on PF approach, to simulate the microstructure evolution of materials at nanoscales. They simulated the morphology of microcrack propagation in single crystal materials under tensile strain with a fixed grip condition, by coupling phase field crystal with an external field method.

The central idea of the phase field approach of brittle fracture consists of regularizing the sharp crack topology within a diffusive crack zone of width l, see Fig. 5, where the regularization of the sharp crack representation is depicted. Therefore, it is possible to define a scalar-valued function that accounts for the stiffness degradation such that $\mathfrak{d}$, with $\mathfrak{d} : \Omega_0^{loc} \times [0, t] \rightarrow [0, 1]$, refer[175,176] for further details.

Within the framework of brittle fracture[211,214,215], the potential energy function for a cracked body can be defined as the sum of the deformation strain energy $\Psi(\mathbf{E})$ integrated over the domain Ω_0^{ph} and the critical fracture energy $\mathcal{G}_c$

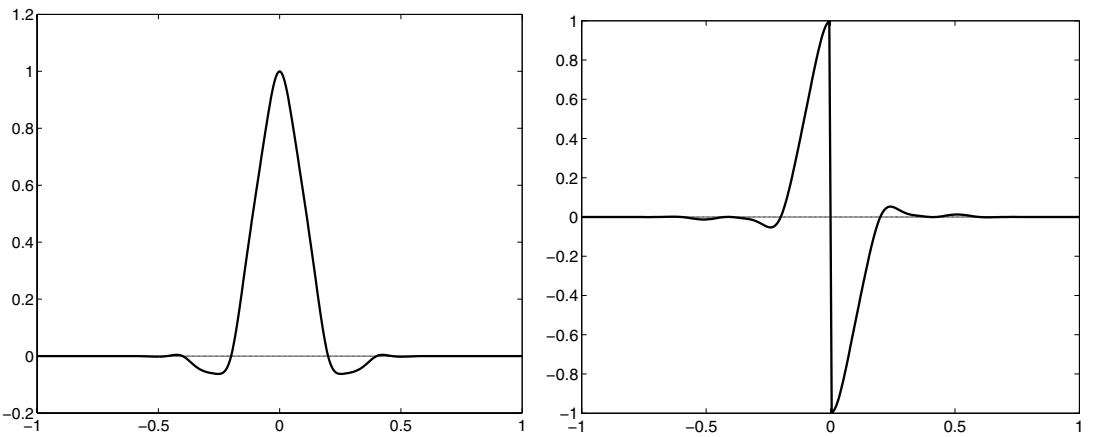

Figure 4: Shape functions in **a** the continuous domain and **b** the discontinuous domain. Picture reproduced with permission from[42].

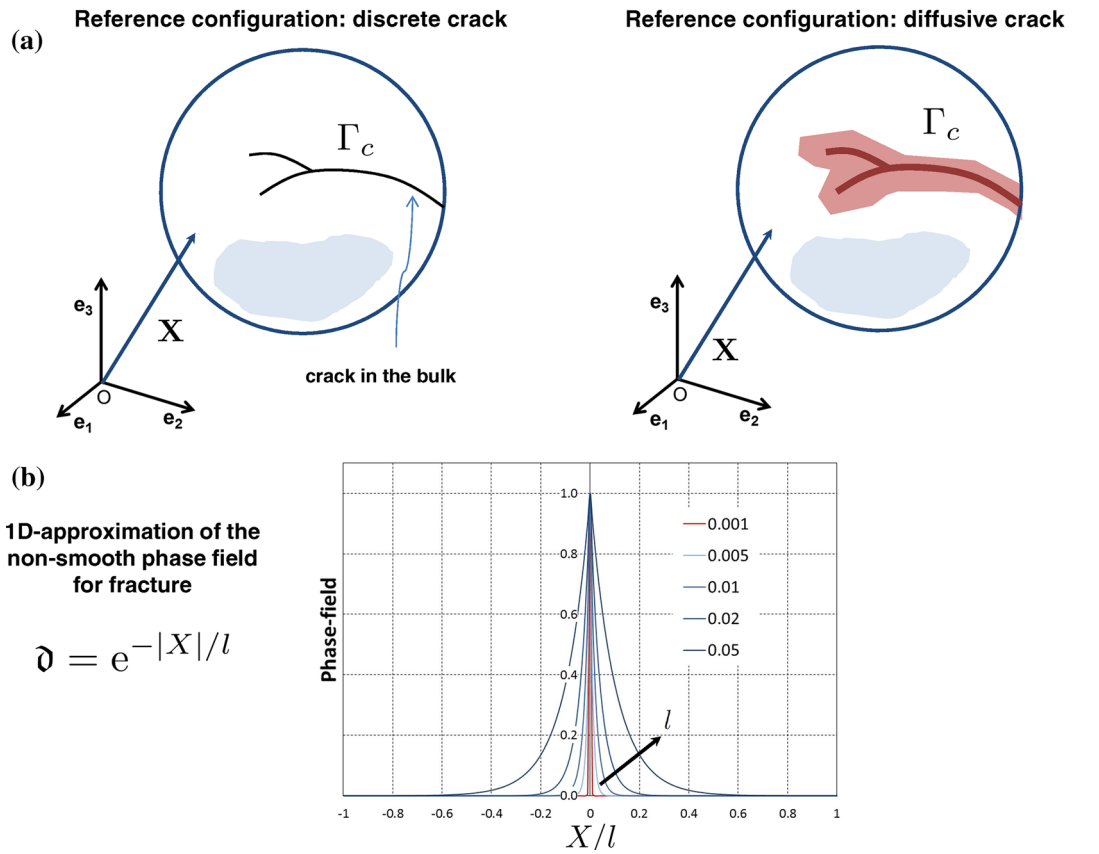

Figure 5: **a** Sharp and diffusive crack modeling. Left: discrete crack discontinuity in the continuum domain. Right: smeared discontinuity in the continuum domain based on the PF approach. **b** Diffusive crack modeling solution for the one-dimensional crack problem.

integrated along the crack path Γ_c, which can be expressed as

$$\Pi(\mathbf{u},\mathfrak{d}) = \int_{\Omega_0^{loc}} \mathfrak{g}(\mathfrak{d})\Psi(\mathbf{E})\,\mathrm{d}\Omega_0^{loc} + \int_{\Omega_0^{loc}} \frac{\mathcal{G}_c l}{2}\left(\frac{\mathfrak{d}^2}{l^2} + |\nabla_{\mathbf{X}}\mathfrak{d}|^2\right)\mathrm{d}\Omega_0^{loc} + \Pi_{\text{ext}}(\mathbf{u}), \tag{30}$$

where Π_{ext} is the contribution due to the prescribed external actions (from the global level), and $\mathfrak{g}(\mathfrak{d}) = [1-\mathfrak{d}]^2 + \mathcal{K}$ identifies the monotonically decreasing degradation function, $\mathcal{K} \approx 0$ being a residual stiffness parameter.

3.4.1 Finite element formulation

The first variation of Eq. (30) with respect to the independent fields $\mathbf{E}$ and $\mathbf{u}$ is given by[175,176]

$$G^u(\mathbf{u},\delta\mathbf{u},\mathfrak{d}) = G^u_{\text{int}} - G^u_{\text{ext}} = \int_{\Omega_0^{\text{loc}}} \mathfrak{g}(\mathfrak{d})\frac{\partial\Psi}{\partial\mathbf{E}} : \frac{\partial\mathbf{E}}{\partial\mathbf{u}}\delta\mathbf{u}\,\mathrm{d}\Omega_0^{\text{loc}} + \delta\Pi_{\text{ext}}(\mathbf{u}) = 0, \quad \forall\delta\mathbf{u}\in\mathfrak{V}^u, \tag{31}$$

in which

$$G^{\mathfrak{d}}(\mathbf{u},\mathfrak{d},\delta\mathfrak{d}) = \int_{\Omega_0^{\text{loc}}} -2(1-\mathfrak{d})\delta\mathfrak{d}\Psi(\mathbf{E})\,\mathrm{d}\Omega_0^{\text{loc}} + \int_{\Omega_0^{\text{loc}}} \mathcal{G}_c l\left[\frac{1}{l^2}\mathfrak{d}\delta\mathfrak{d} + \nabla_{\mathbf{X}}\mathfrak{d}\cdot\nabla_{\mathbf{X}}(\delta\mathfrak{d})\right]\mathrm{d}\Omega_0^{\text{loc}} = 0, \forall\delta\mathfrak{d}\in\mathfrak{V}^{\mathfrak{d}}, \tag{32}$$

where $\mathfrak{V}^u = \left\{\delta\mathbf{u}\in[H^1(\Omega_0^{\text{loc}})] : \delta\mathbf{u} = \mathbf{0} \text{ on } \partial\mathcal{B}_{0,u}\right\}$ denotes the space of admissible displacement variations, and $\mathfrak{V}^{\mathfrak{d}} = \{\delta\mathfrak{d}\in\mathcal{H}^1(\mathcal{B}_0)\,|\,\delta\mathfrak{d} = 0 \text{ on } \Gamma_c\}$ stands for the space of admissible test functions for the phase field. The second Piola-Kirchhoff stress tensor is defined as $\mathbf{S} := \partial_{\mathbf{E}}\Psi$.

In the global scale, the interpolation of the displacement field ($\mathbf{u}$) along with its variation ($\delta\mathbf{u}$) and increment ($\Delta\mathbf{u}$) using the standard trilinear shape functions can be expressed as

$$\mathbf{u}\approx\mathbf{N}\mathbf{d}, \delta\mathbf{u}\approx\mathbf{N}\delta\mathbf{d}, \text{and } \Delta\mathbf{u}\approx\mathbf{N}\Delta\mathbf{d}. \tag{33}$$

The phase field interpolation ($\mathfrak{d}$), its variation ($\delta\mathfrak{d}$), and increment ($\Delta\mathfrak{d}$) at the element level are

approximated using the same shape functions corresponding to the kinematic field:

$$\mathfrak{d} = \mathbf{N}\bar{\mathfrak{d}}, \quad \delta\mathfrak{d} = \mathbf{N}\delta\bar{\mathfrak{d}}, \quad \text{and} \quad \Delta\mathfrak{d} = \mathbf{N}\Delta\bar{\mathfrak{d}}. \tag{34}$$

The gradient of the phase field ($\nabla_{\mathbf{X}}\mathfrak{d}$), its variation ($\nabla_{\mathbf{X}}\delta\mathfrak{d}$), and increment ($\nabla_{\mathbf{X}}\Delta\mathfrak{d}$) are interpolated through a suitable operator $\mathbf{B}^{\mathfrak{d}}$, as mentioned below:

$$\nabla_{\mathbf{X}}\mathfrak{d} = \mathbf{B}^{\mathfrak{d}}\bar{\mathfrak{d}}, \quad \nabla_{\mathbf{X}}\delta\mathfrak{d} = \mathbf{B}^{\mathfrak{d}}\delta\bar{\mathfrak{d}}, \quad \nabla_{\mathbf{X}}\Delta\mathfrak{d} = \mathbf{B}^{\mathfrak{d}}\Delta\bar{\mathfrak{d}}. \tag{35}$$

Applying the displacement and the phase field discretization at the local level to Eqs. (31)–(32) and performing the consistent linearization of the residual vectors, a coupled system of equations can be obtained:

$$\begin{bmatrix} G^{u}(\mathbf{u}, \delta\mathbf{u}, \mathfrak{d}) \\ G^{\mathfrak{d}}(\mathbf{u}, \mathfrak{d}, \delta\mathfrak{d}) \end{bmatrix} \overset{!}{=} \mathbf{0}. \tag{36}$$

3.5 Phantom node method

In the phantom node method (PNM)[166–169], when an element is completely cut by a crack, the displacement field can be represented as continuous on each part of the cracked element and discontinuous across the crack surface. Therefore, the crack kinematics can be obtained by overlapping elements[168–172] using the extra nodes known as phantom nodes. Therefore, (1) the displacement field is discontinuous across the crack but independently continuous on each part of the cracked element. Hence, the discontinuous element is replaced by two elements with the additional phantom nodes, which requires only a small modification in existing finite element codes; (2) the associated shape functions in a cracked element are the same as the shape functions of an intact element, and (3) the elements adjacent to the cracked elements do not require any modification. Because of the above advantages, the computer implementation of the phantom node method is particularly easy.

Consider an arbitrary continuous body with a surface of discontinuity Γ_c. According to the phantom node method[170], the kinematics of a cracked element can be described by superimposing two separate displacement fields, which are active only in a determined region of the domain. Consequently, a completely cut element can be represented as an union: $\Omega_0^{\text{elem}} = \Omega_0^{\text{elem1}} \cup \Omega_0^{\text{elem2}}$, of two elements separated along the crack surface, see Fig. 6a–b. The superscript 'elem' refers to the considered phantom element and 'elem1' and 'elem2' denotes the sub elements after splitting. This formalism is expressed by setting that the crack surface divides the continuum domain into two sub-domains $\Omega_0 = \Omega_{0(+)} \bigcup \Omega_{0(-)}$. Correspondingly, two phantom domains are defined: $\Omega_0^{\text{p}} = \Omega_{0(+)}^{\text{p}} \bigcup \Omega_{0(-)}^{\text{p}}$. Since the elements in the two sub domains do not share any nodes in common, their displacements are independent, resulting in the expected discontinuity across the cross surface.

Through the definition of f as the signed distance measured from the crack surface, W_0^+, W_{p}^-, W_0^-, and W_{p}^+ as the nodes belonging to $\Omega_{0(+)}$, $\Omega_{0(-)}^{\text{p}}$, $\Omega_{0(-)}$, and $\Omega_{0(+)}^{\text{p}}$, respectively, the discontinuous interpolation of the displacement field is given by

$$\mathbf{u}(\mathbf{X}, t) = \sum_{I \in \{W_0^+, W_{\text{p}}^-\}} \mathbf{u}_I(t) N_I(\mathbf{X}) H(f(\mathbf{X})) + \sum_{J \in \{W_0^-, W_{\text{p}}^+\}} \mathbf{u}_J(t) N_J(\mathbf{X}) H(-f(\mathbf{X})), \tag{37}$$

where H is the Heaviside function. In line with[167,219], the standard approximation of the displacements on each part of the cracked element $\Omega_{0(+)}$ and $\Omega_{0(-)}$, which are extended to their corresponding phantom domains $\Omega_{0(-)}^{\text{p}}$ and $\Omega_{0(+)}^{\text{p}}$ introduces the continuous displacement field. The displacement jump between the two flanks of the crack can be computed by taking the difference of the displacement fields of the two domains of the cracked element.

4 Coupling techniques

In this section, we present the techniques to couple the coarse- and fine-scale domains. Two popular techniques, bridging scale method (BSM) and bridging domain method (BDM) to couple the continuum with atomistic domains are discussed.

4.1 Bridging scale method

An overview of the multiscale method based on the bridging scale concept is presented in[220] with an emphasis on complex material systems. In this section, an outline of a three-dimensional multiscale method based on enhanced bridging scale method to model fracture is presented.

Consider a three-dimensional multiscale model shown in Fig. 7 for the adaptive simulation of crack growth. The MD model in Fig. 7a assumes Silicon in the fine-scale domain. The material of the coarse-scale region is modeled based on a solid-shell as shown in Fig. 7b. In the diamond cubic lattice structure of Silicon shown in Fig. 7c, each atom possesses four nearest neighbors. Fig. 7b shows the modeling details of the coarse-scale region highlighting the estimation

of stiffness matrix of a solid shell element. The phantom node method[170] can be used to model the crack surfaces in the coarse-scale region.

Crack originates from the coarse-scale region and the crack tip is captured in the fine-scale region. In Fig. 7a, c, the fine-scale region is formed by the atomistic model, made up of diamond cubic lattice structure of Silicon. Various techniques to model the fine-scale domain are summarized in Sect. 2. The initial crack in the fine-scale region is created by deleting the bonds between the atoms on the crack surface and updating the neighbor list accordingly. Ghost atoms located on the boundary of the coarse region, but within the cutoff radius of the atoms in the fine region (see Fig. 7a), are used to enforce the boundary conditions for the fine-scale solution. A finite-discrete element method combining the advantages of both the finite element method and the discrete element method, coupling by means of ghost particles, is discussed in[221].

In the two-scale model, the total displacement field $\mathbf{u}_\alpha$ of an atom α is decomposed into coarse- and fine-scale components:

$$\mathbf{u}_\alpha = \mathbf{u}_\alpha^{\mathrm{C}} + \mathbf{u}_\alpha^{\mathrm{A}}, \tag{38}$$

where $\mathbf{u}_\alpha^{\mathrm{C}}$ is the coarse-scale component and $\mathbf{u}_\alpha^{\mathrm{A}}$ is the fine-scale component. The fine-scale component $\mathbf{u}_\alpha^{\mathrm{A}}$ is the difference between the actual position of an atom α and the interpolated position of the coarse scale. Therefore, $\mathbf{u}_\alpha^{\mathrm{A}}$ is insignificant in the regions far away from the crack tip, and hence, $\mathbf{u}_\alpha^{\mathrm{C}}$ is sufficient to model the deformation in the coarse-scale region. On the other hand, in the fine-scale region, both coarse- and fine-scale components are required. Let the coarse-scale (see Sect. 3) displacement $\mathbf{u}_\alpha^{\mathrm{C}}$ of an atom α be represented by a set of FEM basis functions defined over a set of n^{C} nodal points,

$$\mathbf{u}_\alpha^{\mathrm{C}} = \sum_{I=1}^{n^{\mathrm{C}}} N_I(\mathbf{X}_\alpha)\mathbf{u}_I^{\mathrm{C}}, \tag{39}$$

where $N_I(\mathbf{X}_\alpha)$ is the shape functions defined at node I, estimated at the αth atom with the material coordinate $\mathbf{X}_\alpha$, and $\mathbf{u}_I^{\mathrm{C}}$ is the continuum displacement vector at node I.

In the bridging scale method, the coupling conditions are realized by enforcing the displacement boundary conditions on the ghost atoms, see Fig. 8. The positions of the ghost atoms are interpolated from the coarse-scale solution. Let β be the index of the ghost atoms; the corresponding ghost atom displacements are estimated as

$$\mathbf{u}_\beta^{\mathrm{C}} = \sum_{I=1}^{n^{\mathrm{C}}} N_I(\mathbf{X}_\beta)\mathbf{u}_I^{\mathrm{C}}, \tag{40}$$

where $N_I(\mathbf{X}_\beta)$ are the shape functions defined at node I, estimated at the βth atom with material coordinates $\mathbf{X}_\beta$.

The bridging scale method has been applied to study various physical phenomenon. A mesoscopic bridging scale (MBS) method, multiscale

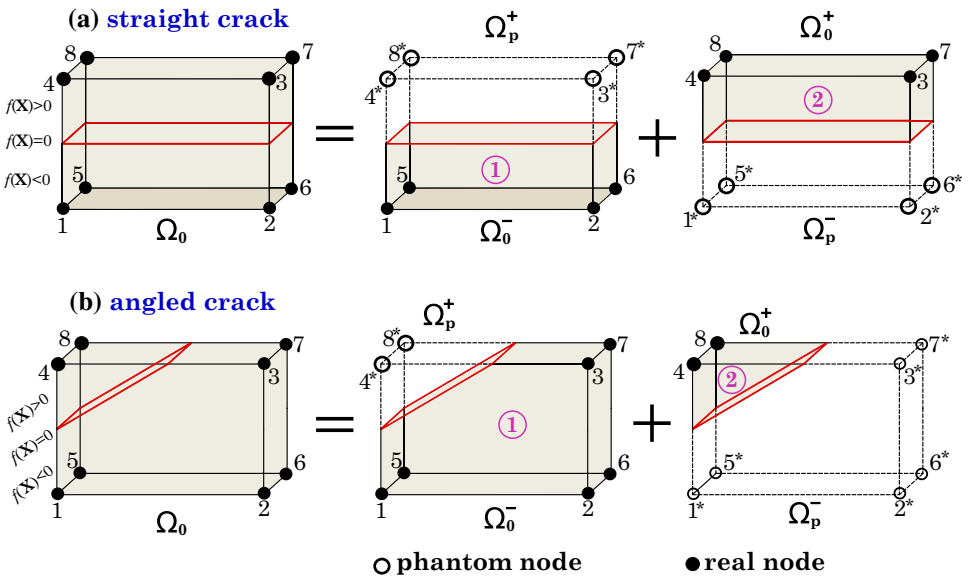

Figure 6: Schematic representation of a cracked element using the phantom node method, for a **a** straight and **b** angled cracks.

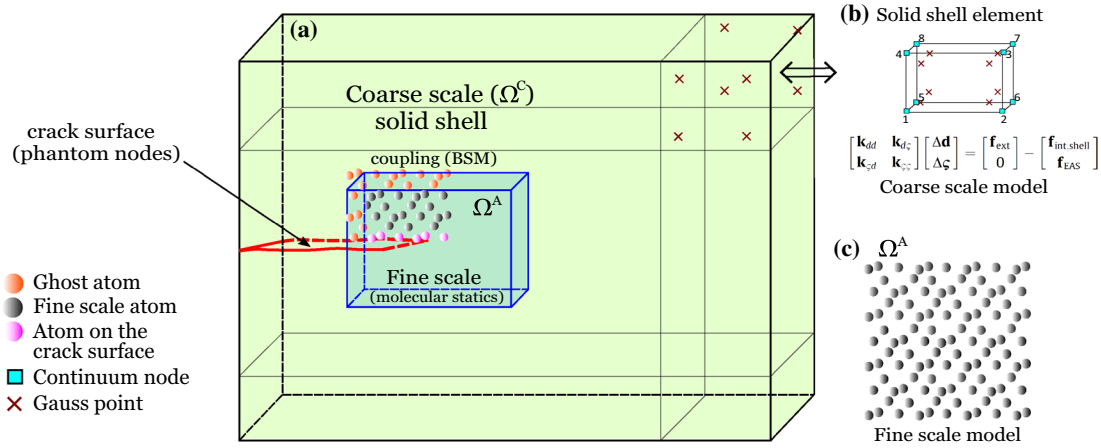

Figure 7: **a** Schematic of a three-dimensional coupled continuum-atomistic model. **b** Mechanics of coarse-scale domain modeled with solid shell element. **c** Fine-scale region showing the arrangement of atoms in the diamond cubic lattice structure of Silicon. Pictures reproduced with permission from[70].

procedure to couple a mesoscale discrete particle model and a macroscale continuum model to study the incompressible fluid flow, is proposed in[222]. Li et al.[223] developed a similar multiscale model, by combining the discrete element method (DEM) at micro scale and Cosserat continuum modeling using the finite element method at macro scale, to simulate dynamical responses in geo-structures composed of granular materials. A bridging scale method is reported in[224], for the analysis of localization problems. The micropolar-continuum model is used to describe the localized deformation in a small number of localized regions. A mathematical framework of the bridging scale method and the time history kernel technique to impose the dynamic interfacial boundary conditions are discussed in[225]. Farrell et al.[35] employed the bridging scale method (BSM) to study intersonic crack propagation, including the formation of a daughter cracks and the sudden acceleration of the crack to a velocity exceeding the material shear wave speed. They also proposed the non-reflecting boundary conditions which can adequately dissipate the strongly localized wave formed by the Mach cone after the crack accelerates beyond the material shear wave speed. The implementation algorithms as well as the development of a time history kernel (THK) for the non-reflective interface are discussed. A BSM-based model coupling the space–time Finite Element Method with MD is developed in[124] to simulate dynamic crack growth. A continuum-based sensitivity analysis of two-dimensional continuum-atomistic models using the bridging scale method is performed in[226]. The authors correlated the influence of material and size variables on the impact of design changes at the macroscopic level to the responses at the atomistic level.

However, extending the BSM to study dynamic crack growth by adaptively adjusting the fine-scale domain and simultaneously avoiding spurious wave reflections at the 'artificial' interface is problematic. Budarapu et al.[12] have developed an adaptive multiscale method (AMM) to concurrently couple the atomistic domain with continuum by enhancing the bridging scale method, to study crack propagation. They modeled the coarse region based on the VAC model and employed PNM to model crack in the coarse region. Furthermore, a meshless adaptive multiscale method for fracture (MAMMF) has been reported in[42], by coupling the atomistic domain with DRKPM-based meshless method in the continuum. Due to the absence of mesh in the continuum, complex fracture patterns can be captured with ease in the MAMMF. Recently, a solid-shell based three-dimensional concurrently coupled adaptive multiscale method has been introduced in[70], to investigate the crack growth in thin-walled structures.

4.2 Bridging domain method

Belytschko and Xiao[6,7] have introduced the bridging domain method for coupling the molecular mechanics (molecular models at zero temperature) and continuum models based on a domain decomposition technique. Coupling in the BDM happens over a definite region (see Fig. 1c), known as 'handshake' domain. Unlike the BSM, in the BDM, the continuum region does not exist

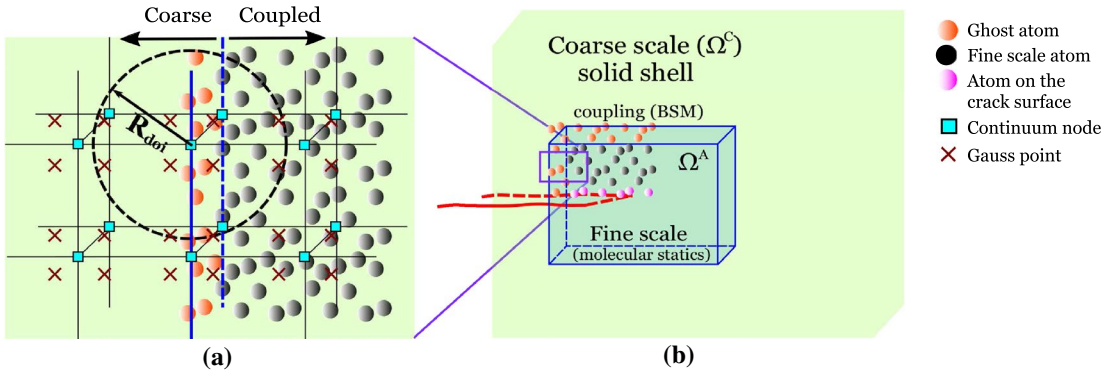

Figure 8: Schematic showing a close up of the region along the coupling boundary. Pictures reproduced with permission from[70].

in the atomistic domain. Second, in the BDM, coupling between the atomistic and continuum regions is based on a linear energy weighting in the bridging domain and is enforced by Lagrange multipliers. Therefore, the total energy of the system is a weighted contributions of the fine and coarse models in the bridging domain. This is achieved through a scalar weight function, w shown in Fig. 9, which is defined as unity outside, zero inside, the fine-scale domain and varies smoothly in the blending region[6]:

$$w = \begin{cases} 1 & \forall \mathbf{X} \in \Omega^{\mathrm{C}} \backslash \Omega^{\mathrm{A}} \\ [0,1] & \forall \mathbf{X} \in \Omega^{\mathrm{B}} \\ 0 & \forall \mathbf{X} \in \Omega^{\mathrm{A}} \backslash \Omega^{\mathrm{C}} \end{cases}, \tag{41}$$

where $\Omega^{\mathrm{C}}, \Omega^{\mathrm{B}}$, and Ω^{A} correspond to the continuum, bridging, and fine-scale domains, respectively. At any point $\mathbf{X}$ in the bridging domain, w can be computed by a normalized distance function:

$$w = \frac{l(\mathbf{X})}{l_0}, \tag{42}$$

where $l(\mathbf{X})$ is the orthogonal projection of $\mathbf{X}$ on the interior boundary of the coarse domain Ω^{C} and l_0 is the length of this orthogonal projection to the boundary of the fine scale Ω^{A}, refer to Fig. 9.

The governing equations of the coupled model are derived from the Hamiltonian of the coupled system, H, which is the sum of the Hamiltonians of each sub-domain:

$$H = (1 - w)H^A + wH^C, \tag{43}$$

where H^{A} and H^{C} are the Hamiltonians of the fine- and coarse sub-domains, estimated as the total potential of coarse- and fine-scale domains. In the BDM, Lagrange multiplier method is employed to constrain the coarse- and fine-scale domain in the bridging region Ω^{B}. In other words, in the handshake region the fine-scale displacements must conform coarse-scale displacements. Therefore, considering the Lagrange multipliers, the total Hamiltonian can be written as

$$H_{\mathrm{L}} = H + \boldsymbol{\lambda}^T \mathbf{g}, \tag{44}$$

where λ is Lagrange multipliers vector and $\mathbf{g}$ is the gap vector between coarse- and fine-scale displacement. Derivation of explicit equations of motion for specific problems are explained in several articles, see[6,7,10,11,36,39,43,227,228].

Belytschko et al.[229] extended the BDM to couple continua with molecular dynamics, where the authors demonstrated the robustness of the methodology by avoiding spurious wave reflections at the molecular–continuum interface. A concurrent multiscale approach based on multigrid principles intended to solve large molecular dynamics systems is attempted in[230]. The authors estimated the effective stiffness matrix of the coarse model by variational restriction of the effective stiffness matrix of the atomistic model. The influence of the time step and the discretization of Lagrange multipliers on spurious wave reflection are investigated in[231] by including a damping term in the fine-scale equations of motion. Guidault et al.[36,227] have enhanced the BDM by also enforcing the strain compatibility between the "atomistic" and continuum domains in the bridging domain, which can be useful for the development of error estimators to drive the adaptive refinement of the coarse scale. However, little gain in accuracy is reported compared to the much simpler L^2 coupling. Xu et al.[232] studied the influence of the enforced constraints through Lagrange multipliers by modeling (1) exact non-diagonal Lagrange multiplier equations and (2) a diagonalized constraint form. Note that

the consistent constraint form conserves linear momentum, angular momentum, and energy, whereas the diagonalized constraint form dissipates energy. Therefore, the diagonalized form is reported to be effective in suppressing spurious reflections at the interface. A variant of the BDM for composite lattices through a 'relaxed' bridging domain method is discussed in[233], where the atom set is divided into primary and secondary atoms, and only the primary atoms are constrained in the coupling region. This will allow the internal modes of the composite lattice to be relaxed, otherwise suppressed by the homogeneous continuum displacement field in the coupling region.

Gracie et al.[10] have extended the BDM for the modeling of dislocations and cracks based on a multiscale atomistic/continuum models. Furthermore, they extended the multiscale model to develop an adaptive concurrent multiscale method[228] for the dynamic simulation of dislocations. Anciaux et al.[234] have developed a BDM-based multiscale method to study the contact area evolution of rough surfaces under normal loading which can lead to the emergence of a strong temperature gradient in the bridging zone. A generalized bridging domain method is introduced in[235], based on independent weight functions to weight the material properties in the coarse- and fine-scale regions, followed by the force equilibrium through imposing compensation forces estimated by force and displacement compatibility requirements. They tested the methodology on a coupled continuum and discrete elements model.

5 Fracture criteria and coarse graining

A fracture criterion should determine whether a crack propagates/nucleates. It should furthermore provide the orientation and "length" of the crack advancement, apart from whether or not cracks branch or join. Considering the non-linearities and non-homogeneities around the crack tip, estimating all the above details based on continuum techniques alone is difficult, particularly when the "length" and direction of crack growth are not controlled[66]. This is because the fracture criterion is often satisfied at several quadrature points in front of the crack tip, and reliable criteria to estimate branching cracks are still missing. Considering the approaches based on configurational forces[236–239], the four major cracking criteria in LEFM are[66] (1) Maximum hoop stress criterion or maximum principal stress criterion. (2) Minimum strain energy density criterion[240]. (3) Maximum energy release rate criterion[241].

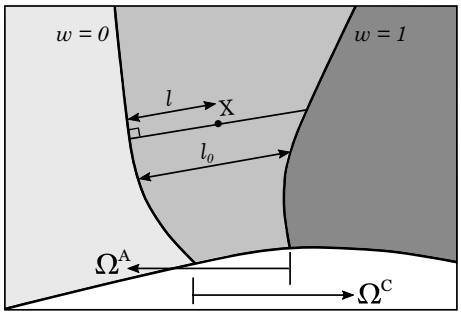

Figure 9: The weight function in the handshake domain in two dimensions.

(4) The zero K_{II} criterion (Vanishing in-plane SIF (K_{II}) in shear mode for infinitesimally small crack extension)[242].

In the multiscale methods mechanics of crack growth around the crack tip are captured in the fine-scale region. Considering the atomistic based multiscale methods, the crack growth is identified based on the distance between the atoms. The orientation and branching are arrived by following the path of the atoms on the crack surface. This information is passed back to the coarse scale. Therefore, estimating the "length" and orientation of crack growth and branching/joining cracks is more accurate and relatively easy in multiscale methods. A two-scale approach to simulate degradation and failure in polycrystalline materials is proposed in[243], where the macro-continuum is modeled using a three-dimensional boundary element formulation in which the presence of damage is formulated through an initial stress approach to account for the local softening in the neighborhood of points experiencing degradation at the micro-scale. The two scales are coupled by transferring the macro-strains to the micro-scale as periodic boundary conditions, while overall macro-stresses are obtained as volume averages of the micro-stress field.

To improve the computational efficiency, the fine-scale region is adaptively adjusted as the crack propagates. The adaptivity scheme consists of adaptive refinement and coarse-graining operations. In order to activate the adaptivity algorithm, the position of the crack tip in the fine-scale region (Ω^A) needs to be estimated. In multiscale methods, when atomistic models are used in the fine-scale region, the atoms on the crack surface are commonly identified based on the energy criteria[10] or centro symmetry parameter (CSP)[42,244,245]. The crack tip is the 'meeting point' of atoms on either side of a crack surface[12]. Subsequently, crack growth is monitored

by comparing the location of the crack tip, in the previous load step to the current load step.

5.1 Energy criteria

The total potential energy of an atomistic system is estimated as the sum of all bond potentials ϕ_α. According to Eq. (4), the bond potential of a particular atom depends on the distance between the atom (α) and its neighbors (β)[10]. In the initial configuration, all the atoms are assumed to possess the same potential energy. The initial crack is created by deleting the bonds between the atoms and updating the neighbor list accordingly. Continuous increase in the external load leads to the stretching of the bonds of the atoms around the crack tip. Increase in bond length/distance between the atoms leads to increase in the system potential energy. A bond breaks when the bond length reaches a certain threshold, transferring the load to the immediate neighbors, see[97] for further details of bond elongation and rotation in an initially notched Graphene system.

Therefore, the atoms around the crack tip possess the highest energy in the entire lattice. This is in agreement with the continuum theory as well, where the stress concentration is observed around the crack tip. Hence, potential energy provides an indication of the location of the crack tip. The energy criterion has been successfully applied to detect the locations of the crack tip[12] and the core of the dislocation[228]. Let $\mathcal{E}_n^{\mathrm{HE}}$ be the set of elements containing at least one atom with high potential energy, i.e.

$$\mathcal{E}_n^{\mathrm{HE}} = \{e \in \mathcal{E}_n^{\mathrm{A}} \mid \text{energy of an atom in } e > \mathrm{tol}^{\mathrm{E}}\}, \tag{45}$$

where $\mathcal{E}_n^{\mathrm{A}}$ is the set of total atoms and $\mathrm{tol}^{\mathrm{E}}$ is the specified energy tolerance. As a guideline, $\mathrm{tol}^{\mathrm{E}}$ can be specified in the range of 15 and 30% higher than the energy of an atom in equilibrium in a perfect lattice.

5.2 Centro symmetry parameter (CSP)

The centro symmetry parameter of an atom α is defined as follows[76]:

$$\mathrm{CSP}_\alpha = \sum_{\beta=1}^{n^{\mathrm{nb}}/2} |\mathbf{r}_{\alpha\beta} + \mathbf{r}_{\alpha(\beta+n^{\mathrm{nb}}/2)}|^2, \tag{46}$$

where $\mathbf{r}_{\alpha\beta}$ and $\mathbf{r}_{\alpha(\beta+n^{\mathrm{nb}}/2)}$ are the distance between the atoms α and β and α and $(\beta + n^{\mathrm{nb}}/2)$, respectively, and n^{nb} are the total number of nearest neighbors of atom α. Consider an atom α in the fine-scale region containing face-centered cubic (fcc) lattice structure. Let β denote the neighbors of α. In an fcc lattice structure every atom α is surrounded by 6 nearest neighbors (n^{nb}). Therefore, the CSP of the atom α in the fcc lattice is given by

$$\mathrm{CSP}_\alpha = \sum_{\beta=1}^{3} |\mathbf{r}_{\alpha\beta} + \mathbf{r}_{\alpha(\beta+3)}|^2 \tag{47}$$

From Eq. (47), the CSP of an atom α in the fcc lattice is the summation of square of the total distance between the opposing neighbors. In other words, the CSP of an atom in a periodic perfect lattice structure with symmetric atomic arrangement is zero and the CSP values of the atoms on the defect surface/stacking fault is not equal to zero. This criterion is used to separate the atoms on the crack surface. Normalized CSP values for various defects are listed in Table 1. From Table 1, atoms on the crack surface can be distinguished as the atoms possessing normalized CSP values greater than or equal to 1.6881.

5.3 Adaptivity

To improve the computational efficiency, the fine-scale region is adaptively enlarged with the defect propagation and the region behind the core of the defect (e.g., crack tip) is coarse grained. An adaptive concurrent multiscale methodology has been introduced in[40] to handle the situations in which both macroscopic and microscopic deformation fields strongly interact near the tip of a crack. The method is based on the balance between numerical and homogenization error; while the first type of error states that elements should be refined in regions of high deformation gradients, the second implies that element size may not be smaller than a threshold determined by the size of the unit cell representing the material's microstructure. Adaptive refinement algorithms for 2D peridynamic grids enhancing the concurrent multiscale methods are discussed in[246]. They applied the adaptive grid refinement to study dynamic crack propagation in two-dimensional brittle materials. An adaptive multiscale method coupling the space–time finite element method with molecular dynamics is developed for the simulation of dynamic fracture problems in[124]. Coupling between the fine- and coarse-scale simulation is achieved with the introduction of a projection operator and bridging scale treatment. An adaptive multiscale methodology based on the Hill-Mandellemmainan FE^2 sense is proposed to deal with localized deformations in[247]. The displacement field of the fine-scale model was decomposed into a homogeneous part, fluctuations,

and a cracking part based on additional degrees of freedom the crack opening in normal and tangential directions. Adaptive mesh refinement and coarsening schemes are proposed in[248] for efficient computational simulation of dynamic cohesive fracture. The adaptive mesh refinement consists of a sequence of edge-split operators, whereas the adaptive mesh coarsening is based on a sequence of vertex-removal (or edge-collapse) operators.

The initial size of the fine-scale domain is chosen such that all the mechanics of crack growth particularly around the crack tip are captured. Therefore, the initial domain size should be sufficient to surround the region ahead and behind the crack tip. Furthermore, a large initial domain can lead to higher computational costs and the crack tip may jump out of very small fine-scale domains. Some of parameters that can influence size of the fine-scale region are as follows: (1) type of problem (static/dynamic), geometry and boundary conditions and (2) type and rate of loading and the type of fracture (brittle/ductile). As a rule of thumb, a square domain is recommended: with areas behind and ahead of the crack tip in the range of 20–25% and 80–75% of the total domain size, respectively, which leads to ≈25% of the area behind the crack tip.

Consider a fine-scale domain embedded within the 'boundaries' of the nodes/particles around the crack tip. The refinement algorithm should be activated sufficiently often such that a buffer layer of elements/'regions' is always maintained between the crack tip and the coupling boundary. The 'regions' refer to the area/volume generated by connecting the immediate neighboring particles in meshless methods, such that they resemble the elements in the mesh-based techniques. Second, to ensure that the refinement operation is not activated in the first load step itself, at least one layer of elements/regions is considered between the crack tip and the buffer element layer. Finally, the crack tip element layer is sandwiched by at least one layer of elements/regions in the transverse direction. In other words, the minimum initial fine-scale region satisfying the above conditions is embedded within a 3×3 discretization. Further details and applications to two- and three-dimensional crack growth problems are explained in[12,42,70,245]. The adaptivity scheme consists of an adaptive refinement and coarse-graining operations, as mentioned below:

1. Estimate the region in the coarse-scale domain Ω^{C} to be refined. A refinement operation involves the expansion of the fine-scale region by converting the estimated coarse region into a fine region, Fig. 10.
2. Estimate the region in the fine-scale domain Ω^{A} to be coarsened. In a coarse-graining operation the coarse region is expanded by converting the estimated fine region into a coarse region, see Fig. 11.

In the above steps, when the sizes of the regions refined and coarse grained are similar, the net change in the size of the fine-scale domain is almost zero. As a result, the fine-scale region is adaptively moved with the propagation of the defect.

Table 1: Range of centro symmetry parameter for various defects, normalized by square of the lattice parameter a_0^2.

Defect	$\mathrm{csp}_\alpha/a_0^2$	Range $\Delta\mathrm{csp}_\alpha/a_0^2$
Perfect lattice	0.0000	$\mathrm{csp}_\alpha < 0.1$
Partial dislocation	0.1423	$0.01 \leq \mathrm{csp}_\alpha < 2$
Stacking fault	0.4966	$0.2 \leq \mathrm{csp}_\alpha < 1$
Surface atom	1.6881	$\mathrm{csp}_\alpha > 1$

5.3.1 Adaptive refinement

The major steps of refinement (Fig. 10) procedure are listed for a multiscale method based on an atomistic fine-scale model:

1. Identify the region to be refined (Ω_{ref}).
2. Create and initialize the atoms in Ω_{ref}.
3. Identify and update the newly cracked atoms.
4. Update the fine and coarse-scale regions.

Figure 10a shows the region identified for a refinement operation. The fine-scale region after the refinement is depicted in Fig. 10b. Let the nodes/particles (before a refinement operation) in the fine, coarse, and completely cracked regions be indicated by $\mathcal{P}_n^{\mathrm{A}}$, $\mathcal{P}_n^{\mathrm{C}}$, and $\mathcal{P}_n^{\mathrm{split}}$, respectively. The region containing split elements indicates the completely cracked region. The steps of a refinement operation are summarized as follows:

- Calculate the atoms on the crack surface based on the CSP and store the regions containing the atoms on the crack surface into the set $\mathcal{P}_n^{\mathrm{csp}}$.
- Estimate the neighbours of the regions containing the atoms on the crack surface in $\mathcal{P}_n^{\mathrm{csp}}$ and store them in $\mathcal{P}_{n+1}^{\mathrm{minA}}$.

- Calculate the regions to be refined, $\mathcal{P}_{n+1}^{\text{refine}}$ by removing the fine-scale region $\mathcal{P}_n^{\text{A}}$ from the set $\mathcal{P}_{n+1}^{\text{minA}}$.
- Flag the regions to be refined and increase the atomistic domain by creating the atoms in the flagged elements.
- Initialize the positions of the newly created atoms through interpolation based on the coarse-scale solution.
- Update the fine and coarse regions after a refinement operation. Update the neighbor list ($nlist_{n+1}$) of the fine-scale atoms in the current load step $(n+1)$.
- Identify the newly cracked particles in the fine-scale region and update the split and tip nodes and the nodal connectivity table.

A detailed algorithm of selecting the particles to be refined, initializing the newly created atoms in the region identified for refinement and propagating the crack in the coarse-scale region in a multiscale framework, is explained in[12,42].

5.3.2 Adaptive coarse graining

The major steps for the coarse-graining operation (Fig. 11) are as follows:

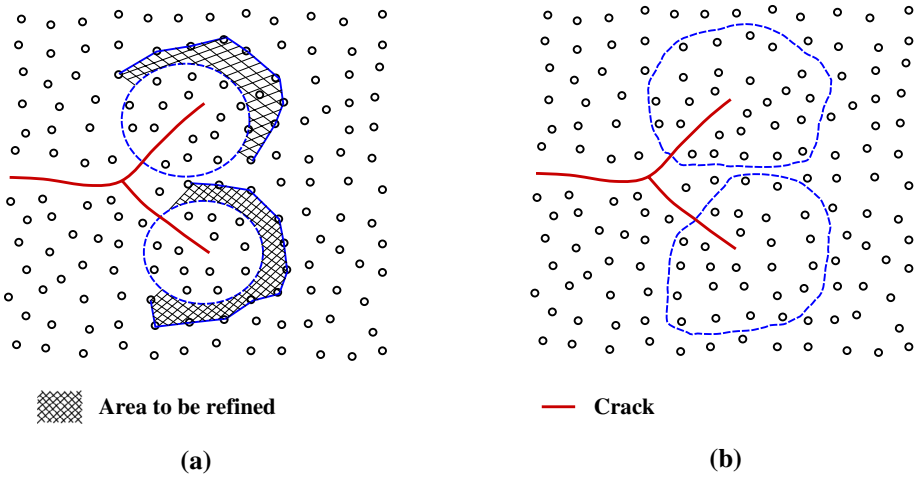

Figure 10: Sketch of the adaptive refinement operation. **a** Flagged particles to be refined are hashed. **b** Increased atomistic region after the refinement operation. Picture reproduced with permission from[42].

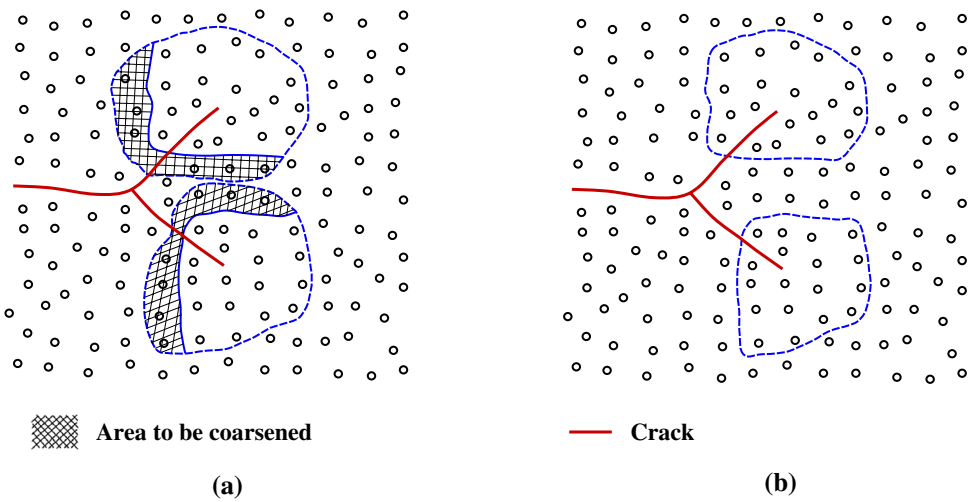

Figure 11: Schematic of the adaptive coarsening operation. **a** Flagged particles to be coarsened are hashed. **b** Reduced atomistic region after the coarsening operation. Picture reproduced with permission from[42].

1. Identify the fine-scale region to be coarse grained (Ω_{coa}).
2. Estimate the equivalent coarse-scale region of Ω_{coa}, refer Sect. 5.4.
3. Delete the atoms in the region to be coarsened.
4. Update the fine- and coarse-scale particles/nodes.

The process of an adaptive coarse-graining operation is explained in Fig. 11. Let $\mathcal{P}_{\mathrm{n}}^{\mathrm{CS}}$ be the regions containing atoms on the crack surface at load step n. Let $\mathcal{P}_{\mathrm{n}}^{\mathrm{BA}}$ be the regions lying in the fine-scale domain and attached to the coupling 'boundary'. The particles/nodes to be coarsened are the particles/nodes which are in both set $\mathcal{P}_{\mathrm{n}}^{\mathrm{CS}}$ and the set $\mathcal{P}_{\mathrm{n}}^{\mathrm{BA}}$ in front of the crack tip, $\mathcal{P}_{\mathrm{n}}^{\mathrm{coarsen}} = \mathcal{P}_{\mathrm{n}}^{\mathrm{CS}} \cap \mathcal{P}_{\mathrm{n}}^{\mathrm{BA}}$. The steps of an adaptive coarsening operation are as follows:

- Estimate and store the regions containing the elements on the crack surface (far away from the crack tip) into $\mathcal{P}_{n}^{\mathrm{LE}}$.
- Find the fine-scale regions attached to the coupling boundary, $\mathcal{P}_{n}^{\mathrm{BA}}$.
- The regions to be coarse grained ($\mathcal{P}_{n+1}^{\mathrm{coarsen}}$) are given by $\mathcal{P}_{n}^{\mathrm{LE}} \cap \mathcal{P}_{n}^{\mathrm{BA}}$.
- Flag the regions to be coarse grained and delete the atoms in the flagged regions.
- Update the particle/nodal set in the fine- and coarse-scale regions and the neighbor list of the fine-scale atoms, after a coarsening operation.

More details can be found in references[12,42].

5.4 Efficient coarse-graining techniques

Upscaling the fracture-related material information from the fine scale to the coarse scale is a major difficulty in multiscale methods for fracture, particularly for complex crack patterns. Belytschko et al.[249] developed a coarse-graining approach named multiscale aggregating discontinuity method. A robust and simple coarse-graining technique in the context of multiscale modeling for fracture is developed by Budarapu et al.[245] The major steps in[245] to develop an equivalent model of the $\Omega_{\mathrm{def}}^{\mathrm{A}}$, the coarse-graining (CG) method (Fig. 12), are as follows:

1. Determine the atoms on the crack surface, e.g., using the CSP.
2. Identify the regions containing atoms on the crack surface, based on the positions of the atoms on the crack surface and the positions of the particles/nodes of the background discretization, see Fig. 12b.
3. Estimate the normal and center of gravity (CoG) of the atoms on the crack surface. Calculate the effective CoG of a crack region by averaging the CoGs of the atoms on the crack surface in the considered crack region.
4. Approximate the crack path in each crack region by joining the effective normal and CoG of the atoms on the crack surface, refer Fig. 12d and Sect. 5.4.1.
5. Estimate the nodes or particles on either side of the crack surface or around the tip, see Fig. 12c.

5.4.1 Crack surface orientation

Consider a deformed configuration of the fine-scale model, superimposed with a discretized coarse-scale model as shown in Fig. 12a. The atoms in the fine region can be separated into small rectangular cells surrounded by four nodes/particles in the coarse region. The center of gravity of a cell containing the atoms on the crack surface can be calculated by averaging the positions of center of gravities of the atoms on the crack surface ($\mathbf{r}_{\alpha}^{\mathrm{cog}}$) in that cell[245]:

$$\mathbf{r}_{\mathrm{cell}}^{\mathrm{cog}} = \frac{\sum_{\alpha=1}^{n^{\mathrm{cacr}}} \mathbf{r}_{\alpha}^{\mathrm{cog}}}{n^{\mathrm{cs}}}, \tag{48}$$

where $\mathbf{r}_{\mathrm{cell}}^{\mathrm{cog}}$ is the approximated position of the center of gravity of the atoms on the crack surface and n^{cs} are the total number of atoms on the crack surface, in a crack region. The normal of the approximated crack surface in the crack region is computed as the average of the normals of the atoms on the crack surface:

$$\mathbf{n}_{\mathrm{cell}}^{\mathrm{cog}} = \frac{\sum_{\alpha=1}^{n^{\mathrm{cs}}} \mathbf{n}_{\alpha}^{\mathrm{cog}}}{n^{\mathrm{cs}}}, \tag{49}$$

where $\mathbf{n}_{\mathrm{cell}}^{\mathrm{cog}}$ is the normal vector of the approximated crack surface in a crack region. Therefore, the crack surfaces in the crack regions are obtained based on the planes passing through $\mathbf{r}_{\mathrm{cell}}^{\mathrm{cog}}$, whose normals are estimated from Eq. (49). Finally, the approximated crack surface in the CG model are obtained by joining the crack surfaces in each crack region.

In order to generate a smooth and continuous crack surface in the CG domain, the start/end positions of the crack surfaces on the vertical edges of the crack regions are averaged, as

illustrated in the schematic Fig. 13. As a rule of thumb, a cell containing at least 12 atoms on the crack surface is observed to be considered as crack region[245]. Therefore, the minimum size of the cell can be adopted as 13 times the lattice parameter. The cell size or the size of fine-scale domain in general could be determined by a-posteriori error estimators. An example of generation of a continuous crack surface in the coarse region is demonstrated in Fig. 13. Consider the vertical edge containing points C, D, E, and F. The points D and E correspond to end points of two crack surfaces and the points C and F are the starting points of new crack surfaces. The largest distance between these points is the distance between the points C and F which is larger than the domain of influence. Thus there exists more than one point on the equivalent crack surface on this particular edge. The total number of points on the equivalent crack surface on this vertical edge can be estimated by recursively checking if the distance between the neighbors of points C, D, E, and F falls within the domain of influence. Figure 14 shows the equivalent coarse-grained model of an atomistic model[245]. The deformed configuration of the atomistic model for a dynamic double edge crack propagation after 108 pico-seconds is shown in Fig. 14a. The corresponding equivalent coarse-grained model is shown in Fig. 14b.

6 Computer implementation

In this section, we discuss the numerical implementation details of a three-dimensional multiscale method for fracture. The atomistic model in the fine region is assumed to be modeled using LAMMPS. The whole computational framework is developed in MATLAB, where the LAMMPS is triggered through `system` command.

6.1 Codes and algorithms

Consider a coarse-scale model implemented in MATLAB coupled to a fine-scale model in the LAMMPS software. Since the LAMMPS software can be triggered from MATLAB, a versatile and robust multiscale strategy can be developed in the MATLAB frame work. To develop such numerical methodology, the `system` command in MATLAB, which triggers an executing system operation, is used as described below[70]:

$$\texttt{system}(\text{'}lmp\_mpi - in \ldots/\ldots/input\_file\_name - loglog.ini\text{'}); \quad (50)$$

where 'lmp_mpi' indicates the LAMMPS executable file generated by compiling the parallel version of the LAMMPS code. The command '.../.../input_file_name' is used to identify the exact location of the input file.

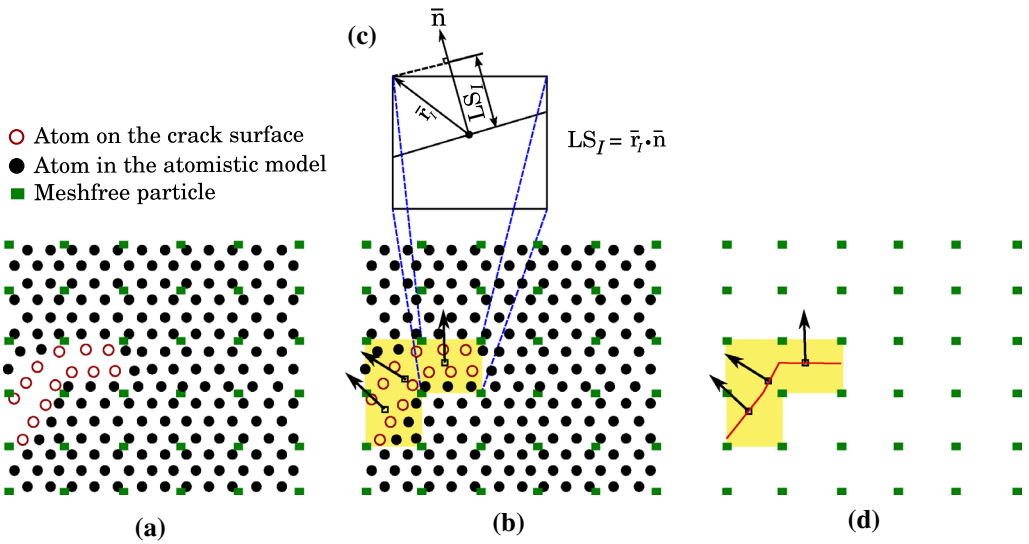

Figure 12: Schematic of meshless equivalent coarse-scale model. **a** Meshfree particles superimposed on the atomistic model, **b** regions containing the atoms on the crack surface are highlighted along with the normals of the crack surface in each region, **c** calculation of level sets and **d** approximation of crack surface by joining the crack path in the regions containing the crack. Picture reproduced from[245] with permission.

6.1.1 Implementation in LAMMPS

Algorithm 1 describes the key steps in a LAMMPS input file to estimate the atom positions through energy minimization. LAMMPS commands are highlighted in blue. The load is assumed to be prescribed in several steps through 'nsteps'(=100) variable, and the atom positions at each load step are estimated based on the minimum energy. 'step_c' indicates the current load step and the amplitude of the displacement in the current step is represented by 'ubary'(=0.05) variable. The atoms in the groups 'top' and 'bot' are uniformly displaced by an amount of 'ubary' through the 'displace_atoms' command. Command 'fix' helps in maintaining the boundary conditions of the specified group of atoms through 'setforce' option, where a 'NULL' value indicates no constraint and '0.0' denote a constraint in that direction. For example, the line "fix 2 top setforce NULL 0.0 NULL", reads

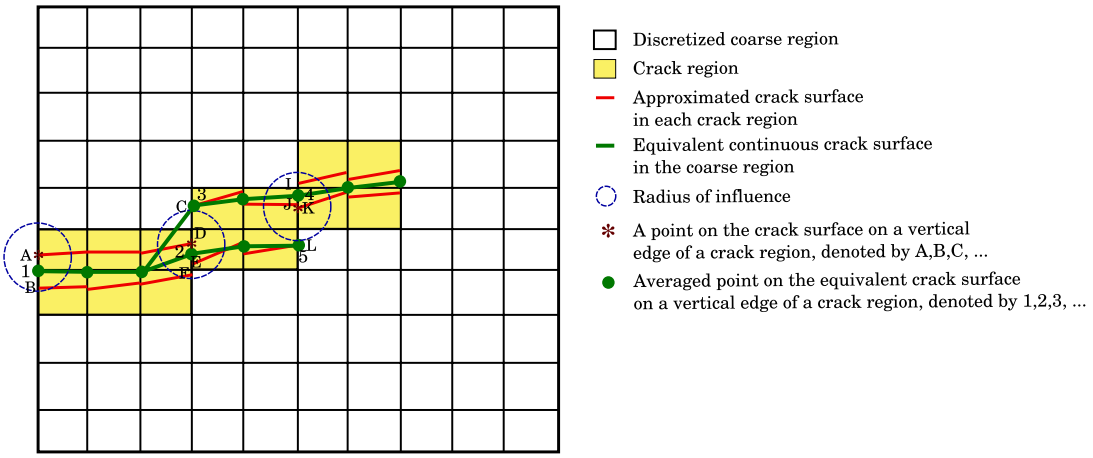

Figure 13: Schematic of averaging the approximated individual crack surface orientation in each crack region, to generate a smooth continuous equivalent crack surface. Picture reproduced from[245] with permission.

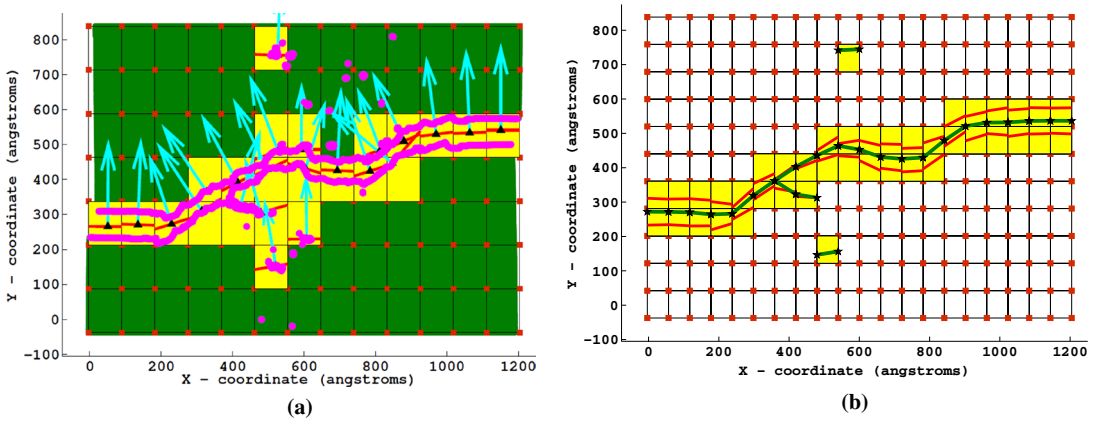

Figure 14: Development of an equivalent coarse-scale model of a given fine-scale model, for a dynamic crack propagation of double edge crack model. **a** Deformed configuration after 108 pico-seconds along with the highlighted atoms on the crack surface, crack regions, and their normals. Approximated crack surface showing the corresponding approximated equivalent crack surfaces. Pictures reproduced from[245] with permission.

as follows: fix number 2, where the 'top' group of atoms are constrained along the '*y*' direction and free to move in the '*x*' and '*z*' directions. Finally, the energy minimization is carried out through the 'minimize' command until the convergence of atom positions within the prescribed limits. The process is repeated in the next load step. The results are stored in the specified file through the 'dump' command before proceeding to the next load step.

```
variable        nsteps  equal   100
variable        step_c  loop    ${nsteps}
variable        ubary   equal   0.05
label           startloop
print           "Iteration = ${step_c}"

# displacing atoms
displace_atoms  top   move  y   ${ubary}   0.0  x  0.0  box
displace_atoms  bot   move  y   -${ubary}   0.0  x  0.0  box

# Fixes
fix  2  top    setforce  NULL   0.0   NULL
fix  3  bot    setforce  NULL   0.0   NULL
fix  4  left   setforce   0.0   NULL   0.0
fix  5  right  setforce   0.0   NULL   0.0

# Minimization
minimize  1.0e-9  1.0e-10  10000  100000
next      step_c
jump      Si_crack.in  startloop
dump   1 all custom 1 dump.Si_${step_c} id type xu yu zu vx vy vz fx fy fz c_pe c_csp
```

Algorithm 1: Key steps of a LAMMPS input file to estimate the atom positions by energy minimization. The load is prescribed in several steps through 'nsteps' variable, and the atom positions at each load step are estimated based on the minimum energy.

Consider the simulation of punching a hole in a rectangular panel through molecular dynamics. This is achieved by specifying a uniform out-of-plane displacement along the *z*-direction to the upper side of the plate in a specific area. Due to symmetry, a quarter of the plate is considered. The hole is punched using a quarter circle with a prescribed radius. The quarter circle is further extruded to a quarter cylinder along the thickness direction. Atoms on the upper side of the quarter cylinder portion are subjected to uniform displacements along the *z*-direction. Figure 15a–c shows the initial and deformed configuration after 100 and 1530 load steps, respectively. The entire material is separated from the plate material after 1530 steps. The evolution of the potential energy versus the strain is plotted in Fig. 16a. The potential energy fluctuates after exceeding a strain of 0.48. The load–displacement curve plotted in Fig. 16b, indicates a corresponding drop in the force. After breaking the initial bonds, the material resisting the external load will be continuously diminishing as the material separation continues.

6.1.2 Multiscale model

The major steps of multiscale model for fracture are summarized in Algorithm 2. The split and tip elements are identified in the discretized domain based on the geometry of the crack(s). This is followed by generating the initial configuration of the atomistic model including initial notches (if applicable). In the third step, a `for` loop applies the boundary conditions on the coarse-scale in several load steps providing the coarse-scale solution $\mathbf{u}_I^C$, in each step. The ghost atom positions are interpolated from the coarse-scale solution using Eq. (40). They are the boundary conditions for the fine scale. The LAMMPS executable can now be triggered again to minimize the potential energy of atomistic domain by fixing the updated ghost atom positions. In each load step, the latest atom positions at the end of the energy minimization along with their energy and centro symmetry parameter (CSP) are stored an output file. The crack tip is identified by using either the energy or the CSP criteria. The adaptivity scheme is activated if the crack tip location is close to the boundary of the atomistic domain.

1. Identify the split and tip elements in the coarse region.
2. Estimate the initial fine scale domain size and the atom positions.
3. **for** *(load_step) i = 1:number of steps* **do**
   (a) Apply the boundary conditions in continuum and solve for the coarse scale solution $\mathbf{u}_I^C$.
   (b) Interpolate the ghost atom positions based on Eq. (40).
   (d) Trigger LAMMPS to execute the updated input file, where potential energy of atomistic domain is minimized by constraining the updated positions of ghost atoms.
   (e) Dump the latest atom positions along with their energy and centro symmetry parameter.
   (f) Estimate the location of the crack tip based on the energy/CSP criteria.
   (g) Activate the adaptivity scheme depending on the location of the crack tip.
end

Algorithm 2: Major steps in the solution algorithm of a multiscale model.

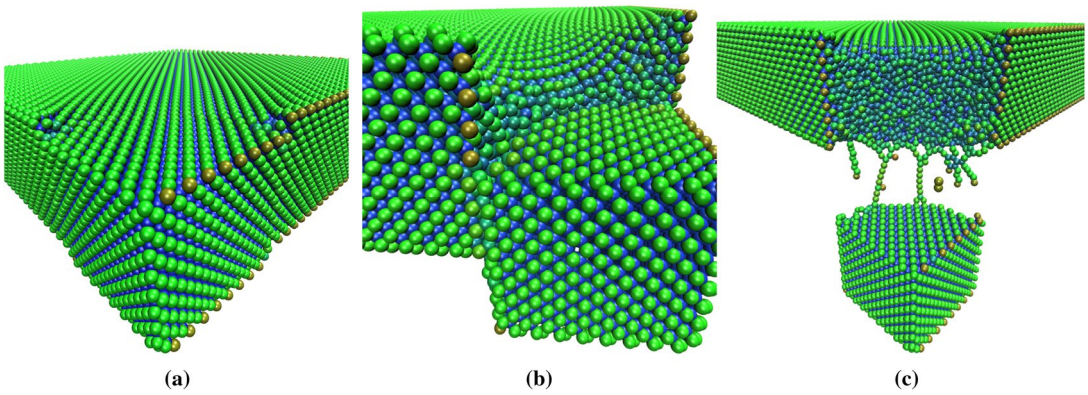

Figure 15: Deformed configurations based on the atomistic model, during punching a hole in Silicon. Distribution of the potential energy at various instances of the punching process. **a** Initial, **b** after 100 load steps, and **c** after 1530 steps. Pictures reproduced with permission from[70].

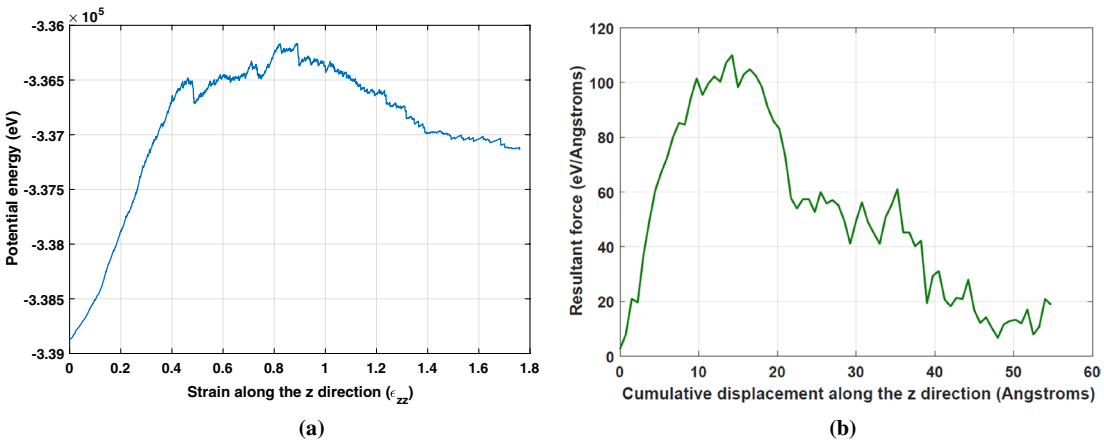

Figure 16: **a** Distribution of the potential energy with strain and **b** load-displacement diagram generated based on the MD simulations of punching a hole in a rectangular panel. Pictures reproduced with permission from[70].

Consider the simulation of Mode I crack growth of two through-the-thickness edge cracks, located in the middle of the plate. The cracks in the coarse-scale domain are modeled by employing the phantom node method. Displacement loads are prescribed on the top and bottom row of atoms. Deformed configurations after 28 and 38 load steps are plotted in Fig. 17a, b, respectively. Cracks propagate in the opposite directions after 28 load steps. Figure 17c shows the coupled model after an adaptive refinement after 39 load steps. Since the available space between the initial fine-scale regions in Fig. 17a is small, the two fine-scale regions are merged in the adaptive refinement. Simultaneously, the adaptive coarsening scheme coarse grains the fine-scale regions behind the crack tips. The deformed configuration of the multiscale model at the end of the simulation is shown in Fig. 17d, where almost a complete merging of the two cracks and hence the separation of the fine-scale region into two parts can be noticed. Some key contributions towards the multiscale methods for fracture in the past two decades are summarized in Table 2.

7 Future prospects and conclusions

Most of the problems in real-time involve multiple field and disparate time and length scales. Based on the significant advancement of the multiscale methods in the past two decades, multiphysics multiscale methods are rapidly growing to simulate fracture in various applications, such as heterogeneous porous medis and/or hydralic fracture[253], polycrystalline[254] and composite materials[255,256] design, batteries[257,258], nano

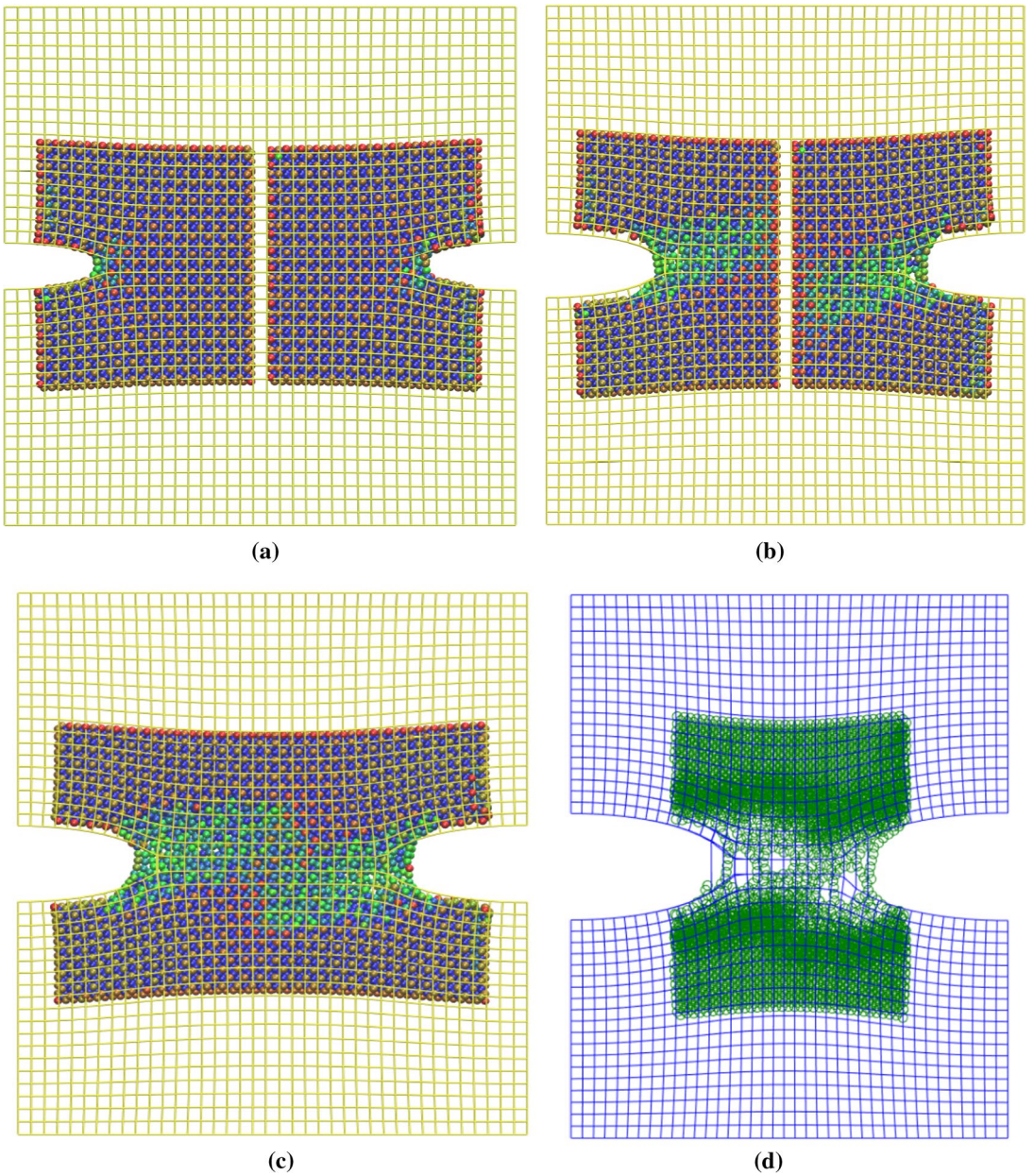

Figure 17: Crack propagation of a double-edge notched specimen. **a** Deformed configuration after 28 load steps. Activation of adaptive refinement and coarse graining of the fine-scale region as the crack grows. **b** Deformed configuration after 38 load steps, before refinement and **c** after an adaptive refinement operation after 39 load steps. Adaptive refinement and coarse-graining algorithms (see[12]) are activated after 39 load steps as the cracks grow. As a result, the two fine-scale regions are merged after 39 load steps and the combined fine-scale region is adaptively coarse grained, as shown in **d**. Pictures reproduced with permission from[70].

materials[259], bio applications[260], to name a few. In this section, we outlined the current status of latest multiscale techniques based on quantum mechanics, peridynamics, and techniques for biological applications, apart from some comments on future prospects.

7.1 Quantum mechanics and molecular mechanics

Estimation of mechanical and fracture properties of the nano scale structures such as carbon nanotubes, two-dimensional materials like Graphene and MoS2 through experiments is

extremely challenging[261]. Hence, as an alternative to experiments, quantum mechanics (QM)based techniques can be primarily employed to predict the fracture, bond breaking, and bond formation in particular[262], and when using the simulation techniques that consider electrons, i.e., quantum modeling is indispensable. In spite of significant progress in the computational resources, the computational expenses of simulations based on QM still remains a challenging task. Therefore, MD simulations are computationally more economical compared to that of QM. However, due to small dimensions of atoms, full-scale atomistic models for day-to-day engineering calculations are prohibitively expensive. In this context, multiscale methods coupling quantum mechanics, molecular mechanics (MM), coarse graining (CG), and continuum mechanics (CM) techniques seem to be efficient, coupling the advantages and surpassing the disadvantages of each technique individually.

ONIOM[263] is a technique coupling QM and MM based on overlapping domain scheme. The basic idea of ONIOM scheme is to apply the coarse-scale model like MM to the entire domain and the more accurate QM-based fine-scale model in the critical regions where bond breaking is expected. A higher order correction, estimated as the difference between the QM and MM energies of the fragment domain, can be applied to cancel the effect of the complete MM model assumption in the coupling domain that is overlapped by the QM model. Therefore, the total energy of the system can be written[263] as follows:

$$E(\mathbf{x}_\alpha, c_\alpha) = E^{\mathrm{MM}}(\mathbf{x}_\alpha) + E_{\mathrm{F}}^{\mathrm{QM}}(\mathbf{x}_\alpha, c_\alpha) - E_{\mathrm{F}}^{\mathrm{MM}}(\mathbf{x}_\alpha), \tag{51}$$

where E^{MM} is the energy of the MM domain, $E_{\mathrm{F}}^{\mathrm{QM}}$ is the energy of the fine-scale sub-domain calculated based on QM, $E_{\mathrm{F}}^{\mathrm{MM}}$ is the energy estimated using MM in the fine-scale region, $\mathbf{x}_\alpha$ is the vector of current atom position, and c_α is the set of basis function coefficients used in the representation of the electronic wave function. On the other hand, the quantum to molecular mechanical overlapping domain (QtMMOD) method[264] requires a partial overlap between the MM and the QM sub-domains. Therefore, the QM model is used in the interesting area, whereas the underlying MM model is employed on the sub-domain excluding the interesting region. In other words, the MM domain does not exist in the entire domain as in the case of ONIOM method. Park et al.[265] propose another multiscale approach by concurrently combining the QM, MM, and CG techniques. They identified two distinct interfaces, MM/CG and QM/MM, where the QM domain does not interact with CG domain and MM and CG regions are coupled by quasi-continuum.

7.2 Peridynamics based multiscale methods

Peridynamics[266–269] is a nonlocal computational formulation of continuum mechanics, equivalent to a coarse-grain model in multiscale perspective. The main difference between the continuum mechanics and the peridynamics is the nonlocal interaction between material points. Consider a fixed material point $\mathbf{r}_\alpha$ in the current configuration, which can interact with neighboring particles $\mathbf{r}_\beta$ within a compact support called as `horizon`, which is similar to the concept of 'domain of influence' in the meshless methods or 'cutoff range' in molecular dynamics. The nonlocal equilibrium equations of motion can be derived by considering the balance of linear momentum at the material point $\mathbf{r}_\alpha$, as mentioned below[180]:

$$\rho_\alpha \ddot{\mathbf{r}}_\alpha = \mathbf{L}(\mathbf{R}_\alpha, t) + \rho_\alpha \mathbf{b}(\mathbf{R}_\alpha), \tag{52}$$

where ρ_α is the average density of the material at point α

$$\mathbf{L}(\mathbf{R}_\alpha, t) = \int_{H_\alpha} (\mathbf{T}_\alpha \langle \mathbf{R}_\beta - \mathbf{R}_\alpha \rangle - \mathbf{T}_\beta \langle \mathbf{R}_\alpha - \mathbf{R}_\beta \rangle) dV_\beta \tag{53}$$

is the nonlocal stress divergence vector acting on the α^{th} material point by neighboring macroscale points β, equivalent to a local divergence term in continuum mechanics[180].

A peridynamics based multiscale method has been developed in[180], using the multiscale micromorphic molecular dynamics (MMMD) theory to couple the molecular dynamics in the fine-scale region. To address the issue of wave reflection on the interface, the authors proposed a filter by turning on and off the MMMD dynamic equations at different scales. A coupled model embedding peridynamics within a molecular dynamics code is available at[270]. A peridynamics based hierarchical multiscale modeling scheme coupling peridynamics with the atomistic model has been employed in[271], to model a complex heterogeneous polymer, ultra high molecular weight polyethylene (UHMWPE). Refer to[179,252] for a multiscale strategy coupling peridynamics with continuum based finite element method. Different methods are compared in[272], to estimate the

Table 2: Key contributions on multiscale methods for fracture based on BSM and BDM techniques.

No.	Address	Title	Comments
1	Wagner et al., J Comp Phy, 190:249–279, 2003	Coupling of atomistic and continuum simulations using a bridging scale decomposition[32]	Introduction to BSM
2	Park et al., Phil Mag, 85:79–113, 2005	The Bridging Scale for Two-Dimensional Atomistic/Continuum Coupling[33]	Wave relections and time history kernel in BSM
3	Tang et al., IJNME, 65:1688–1713, 2006	A mathematical framework of the bridging scale method[225]	Modified interfacial conditions based on THK
4	Farrell et al., IJNME, 71:583–605, 2007	Implementation Aspects of the Bridging Scale Method and Application to Intersonic Crack Propagation[35]	Computer implementation algorithms and shear dominant failure using BSM.
5	Budarapu et al., CMAME, 319:338–365, 2017	Concurrently coupled solid shell-based adaptive multiscale method for fracture[70]	Solid shell-based multiscale method for adaptive crack growth, using BSM.
6	Belytschko et al., CMAME, 193:1645–1669, 2004	A bridging domain method for coupling continua with molecular dynamics[229]	BDM to simulate dynamic fracture.
7	Gracie et al., IJNME, 86:575–597, 2011	Adaptive Continuum-Atomistic Simulations of Dislocation Dynamics[228]	Adaptive XBDM for dislocation dynamics.
8	Talebi et al., Comp Mech, 53:1047–1071, 2014	A Computational Library for Multiscale Modelling of Material Failure[11]	Multiscale framework for 3D dynamic fracture using XBDM.
9	Miller et al., MSMSE, 17:053001, 2009	A unified framework and performance benchmark of fourteen multiscale atomistic/continuum coupling methods[250]	Comparison of accuracy and efficiency of 14 multiscale methods on a test problem.
10	Nair et al., JMPS, 59:2476–2487, 2011	ACoupled quantum-continuum analysis of crack tip processes in aluminum[251]	Coupled quantum-continuum analysis of crack.
11	Liu et al., CMAME, 245:163–175, 2012	A coupling approach of discretized peridynamics with finite element method[252]	Coupled FEM and Peridynamics model.
12	Giovanardi et al., CMAME, 2017	A hybrid XFEM-Phase field (Xfield) method for crack propagation in brittle elastic materials[218]	Coupled XFEM-Phasefield method.

tangent-stiffness matrices in a massively parallel computational peridynamics code.

7.3 Multiscale methods for biological applications

Many biological materials, such as nacre, tooth, and bone are composite materials made up of stiff brittle ceramics and compliant organic materials like polymer. Compared to their constituents, natural organic/inorganic composites exhibit much enhanced strength and toughness properties. Based on this inspiration, several biomimetic composites are proposed in an attempt to synthesize materials with superior mechanical properties. However, most current synthetic composites have not exhibited their full potential of property enhancement compared to the natural prototypes they are mimicking. The main reason being the weak junctions between stiff and compliant phases, which need to be optimized according to the intended functions of the composite material[273].

Investigating biological system mechanics at the smallest scale does not always provide a complete picture[274]. Therefore, understanding the influence of multiphasic interfaces and hierarchical organizations across length scales on macroscale properties in natural systems will help in developing a materials-by-design approach for novel engineering materials, such as nanocomposites with tailored interfaces and programmed microstructures, e.g., the brick-and-mortar arrangement of stiff filler and soft matrix phases observed in nacre[275]. Niebel et al.[276] conducted

experimental and numerical studies to understand the influence of the polymer properties on the mechanics of nacre-like composites containing an intermediate fraction of mineral phase and reported that the stiffer polymers can increase the strength of the composite by reducing stress concentrations in the inorganic scaffold. A finite element based analysis is carried out in[273], to estimate the improvement in the mechanical properties of nacre like biomimetic composites. Awaja et al.[277] summarized the recent developments on the topics of cracks and microcracks initiation and propagation in polymer structures along with the techniques for detection and observation. Moreover, repair of cracks and microcracks through bio-mimetic self-healing techniques is also discussed along with surface active protection.

Mechanisms of energy dissipation in structural molecules at nanoscales can be estimated based on the sacrificial bonds and hidden length (SBHL). The presence of SBHL leads to greater fracture toughness as compared to the materials without such features. The increase in interface toughness as a function of polymer density and number of sacrificial bonds has been investigated in[278], based on the mechanical properties of the polymeric system. Tessellation is a structural motif involving periodic soft and hard elements arranged in series which appears in a vast array of invertebrate and vertebrate animal biomaterials. Tessellation of a hard, continuous surface, connected by a softer phase results in maximization of material toughness, with little expense to stiffness or strength[279].

Dental enamel is a hybrid material consisting of brittle fibers and compliant organic materials like protein matrix. Enamel exhibits high fracture toughness and stiffness due to a complex hierarchical and graded microstructure, optimally organized from nano to macroscale. The deformation and damage behavior of the fibrous microstructure is studied in[280] using a 3D RVE and continuum damage mechanics model coupled to hyperelasticity for modeling the initiation and evolution of damage in the mineral fibers as well as protein matrix. Ural et al.[281] simulated the bone fracture based a multiscale method using cohesive finite elements. A failure mode transition in nacre and bone-like materials has been demonstrated in[282].

To summarize, based on the rapid progress in multiscale methods, the expensive and time-consuming experiments can be avoided in future either completely or partially. Moreover, since the real-time problems involve multiphysics, an interdisciplinary collaboration among different groups is required to accurately predict and understand the physics/mechanics across the scales. This is a good sign, which helps not only to quickly understand the fundamental mechanics of failure, but also to bring in revolutionary changes in the material design and analysis.

Acknowledgements

PRB acknowledge the funding from the European Research Council (ERC), Grant No. 306622 through the ERC Starting Grant "Multi-field and multi-scale Computational Approach to Design and Durability of PhotoVoltaic Modules"—CA2PVM.

Received: 20 January 2017 Accepted: 19 July 2017
Published online: 11 October 2017

References

1. Tadmor EB, Ortiz M, Phillips R (1996) Quasicontinuum analysis of defects in solids. Philos Mag A 73(6):1529–1563
2. Abraham FF, Walkup R, Gao H, Duchaineau M, DeLaRubia TD, Seager M (2002) Simulating materials failure by using up to one billion atoms and the world's fastest computer: work-hardening. Proc Nat Acad Sci 99(9):5777–5782
3. Buehler MJ, Hartmaier A, Gao H, Duchaineau M, Abraham FF (2004) Atomic plasticity: description and analysis of a one-billion atom simulation of ductile materials failure. Comput Methods Appl Mech Eng 193(48–51):5257–5282
4. Liu WK, Su H, Belytschko T, Li S, Chang CT (2000) Multi-scale methods. Int J Numer Methods Eng 47:1343–1361
5. Miller RE, Tadmor EB (2002) The quasicontinuum method: overview, applications and current directions. J Comput Aided Mater Des 9(3):203–239
6. Belytschko T, Xiao SP (2003) Coupling methods for continuum model with molecular model. Int J Multiscale Comput Eng 1(1):115–126
7. Xiao SP, Belytschko T (2004) A bridging domain method for coupling continua with molecular dynamics. Comput Methods Appl Mech Eng 193(17–20):1645–1669
8. Liu WK, Park HS, Qian D, Karpov EG, Kadowaki H, Wagner GJ (2006) Bridging scale methods for nanomechanics and materials. Comput Methods Appl Mech Eng 195(13–16):1407–1421
9. Belytschko T, Loehnert S, Song JH (2008) Multiscale aggregating discontinuities: a method for circumventing loss of material stability. Int J Numer Methods Eng 73(6):869–894

10. Gracie R, Belytschko T (2008) Concurrently coupled atomistic and XFEM models for dislocations and cracks. Int J Numer Meth Eng 78(3):354–378
11. Talebi H, Silani M, Bordas SPA, Kerfriden P, Rabczuk T (2014) A computational library for multiscale modelling of material failure. Comput Mech 53(5):1047–1071
12. Budarapu PR, Gracie R, Bordas SPA, Rabczuk T (2014) An adaptive multiscale method for quasi-static crack growth. Comput Mech 53(6):1129–1148
13. Shenoy VB, Miller RE, Tadmor EB, Rodney D, Phillips R, Ortiz M (1999) An adaptive finite element approach to atomic-scale mechanics-the quasicontinuum method. J Mech Phys Solids 47(3):611–642
14. Beex LAA, Peerlings RHJ, Geers MGD (2011) A quasicontinuum methodology for multiscale analysis of discrete microstructural models. Int J Numer Methods Eng 87:701–718
15. Sun Y, Peng Q, Lu G (2013) Quantum mechanical modeling of hydrogen assisted cracking in aluminum. Phys Rev B 88:104109
16. Beex LAA, Kerfriden P, Rabczuk T, Bordas SPA (2014) Quasicontinuum-based multiscale approaches for plate-like beam lattices experiencing in-plane and out-of-plane deformation. Comput Methods Appl Mech Eng 279:348–378
17. Beex LAA, Peerlings RHJ, Geers MGD (2014) A multiscale quasicontinuum method for lattice models with bond failure and fiber sliding. Comput Methods Appl Mech Eng 269:108–122
18. Hajibeygi H, Karvounis D, Jenny P (2011) A hierarchical fracture model for the iterative multiscale finite volume method. J Comput Phys 230:8729–8743
19. Paggi M, Wriggers P (2012) Stiffness and strength of hierarchical polycrystalline materials with imperfect interfaces. J Mech Phys Solids 60:557–572
20. Paggi M, Corrado M, Rodriguez MA (2013) A multi-physics and multi-scale numerical approach to microcracking and power-loss in photovoltaic modules. Compos Struct 95:630–638
21. Wudtke I, Talebi H, Silani M, Werner F (2015) A hierarchical multi-scale approach to mechanical characterization of heat affected zone in welded connections. Comput Mater Sci 96:396–402
22. Lawrimore WB, Paliwal B, Chandler MQ, Johnson KL, Horstemeyer MF (2016) Hierarchical multiscale modeling of polyvinyl alcohol/montmorillonite nanocomposites. Polymer 99:386–398
23. Lyu D, Fan H, Li S (2016) A hierarchical multiscale cohesive zone model and simulation of dynamic fracture in metals. Eng Fract Mech 163:327–347
24. Feyel F (1999) Multiscale FE^2 elastoviscoplastic analysis of composite structures. Comput Mater Sci 16(1–4):344–354
25. Feyel F, Chaboche JL (2000) FE^2 multiscale approach for modeling the elastoviscoplastic behavior of long fiber sic/ti composite materials. Comput Methods Appl Mech Eng 183:309–330
26. Feyel F, Chaboche JL (2001) Multi-scale non linear FE^2 analysis of composite structures: damage and fiber size effects. In: Saanouni K (ed.) Numerical Modelling in Damage Mechanics - NUMEDAM00. Revue Eur Elem Finis 10:449–472
27. Feyel F, Chaboche JL (2003) A multilevel finite element method (FE^2) to describe the response of highly nonlinear structures using generalized continua. Comput Methods Appl Mech Eng 192:3233–3244
28. Talebi H, Zi G, Silani M, Samaniego E, Rabczuk T (2012) A simple circular cell method for multi-level finite element analysis. J Appl Math. ID: 526846
29. Silani M, Ziaei-Rad S, Talebi H, Rabczuk T (2014) A semi-concurrent multiscale approach for modeling damage in nanocomposites. Theoret Appl Fract Mech 74:30–38
30. Zhu H, Wang Q, Zhuang X (2016) A nonlinear semi-concurrent multiscale method for fractures. Int J Impact Eng 87:65–82
31. Zhuang X, Wang Q, Zhu H (2017) Multiscale modelling of hydro-mechanical couplings in quasi-brittle materials. Int J Fract. doi:10.1007/s10704-016-0139-1
32. Wagner GJ, Liu WK (2003) Coupling of atomistic and continuum simulations using a bridging scale decomposition. J Comput Phys 190(1):249–279
33. Park HS, Karpov EG, Liu WK, Klein PA (2005) The bridging scale for two-dimensional atomistic/continuum coupling. Philos Mag 85(1):79–113
34. Dhia HB (2006) The Arlequin method: a partition of models for concurrent multiscale analyses. In: Challenges in computational mechanics workshop, Cachan, France, 10–12 May, 2006
35. Farrell DE, Park HS, Liu WK (2007) Implementation aspects of the bridging scale method and application to intersonic crack propagation. Int J Numer Methods Eng 71:583–605
36. Guidault PA, Belytschko T (2009) Bridging domain methods for coupled atomistic continuum models with l^2 or h^1 couplings. Int J Numer Methods Eng 77(4–5):1566–1592
37. Broughton J, Abraham FF, Bernstein N, Kaxiras E (1999) Concurrent coupling of length scales: methodology and application. Phys Rev B 60(4):2391–2403
38. Tang S, Kopacz AM, O'Keefe SC, Olson GB, Liu WK (2013) Concurrent multiresolution finite element: formulation and algorithmic aspects. Comput Mech 52(6):1265–1279
39. Talebi H, Silani M, Bordas SPA, Kerfriden P, Rabczuk T (2013) Molecular dynamics/XFEM coupling by a three dimensional extended bridging domain with applications to dynamic brittle fracture. Int J Multiscale Comput Eng 11(6):527–541
40. Vernerey FJ, Kabiri M (2014) Adaptive concurrent multiscale model for fracture and crack propagation

in heterogeneous media. Comput Methods Appl Mech Eng 276:566–588
41. Wu J, Zhang H, Zheng Y (2015) A concurrent multiscale method for simulation of crack propagation. Acta Mech Solida Sin 28(3):235–251
42. Yang S-W, Budarapu PR, Mahapatra DR, Bordas SPA, Zi G, Rabczuk T (2015) A meshless adaptive multiscale method for fracture. Comput Mater Sci 96B:382–395
43. Talebi H, Silani M, Rabczuk T (2015) Concurrent multiscale modeling of three dimensional crack and dislocation propagation. Adv Eng Softw 80:82–92
44. Ghosh S, Lee K, Moorthy S (1994) Multiple scale analysis of heterogeneous elastic structures using homogenization theory and voronoi cell finite element method. Int J Solids Struct 32:27–62
45. Kouznetsova V, Geers MGD, Brekelsmans WAM (2002) Multi-scale constitutive modeling of heterogeneous materials with a gradient-enhanced computational homogenization scheme. Int J Numer Methods Eng 54:1235–1260
46. Guidault PA, Allix O, Champaney L, Navarro JP (2007) A two-scale approach with homogenization for the computation of cracked structures. Comput Struct 85:1360–1371
47. Özdemir I, Brekelmans WAM, Geers MGD (2008) FE^2 computational homogenization for the thermo-mechanical analysis of heterogeneous solids. Comput Methods Appl Mech Eng 192:602–613
48. Verhoosel CV, Remmers JJC, Gutiérrez MA, de Borst R (2010) Computational homogenization for adhesive and cohesive failure in quasi-brittle solids. Int J Numer Methods Eng 83(8–9):1155–1179
49. Nguyen VP, Lloberas-Valls O, Stroeven M, Sluys LJ (2011) Homogenization-based multiscale crack modelling: From micro-diffusive damage to macro-cracks. Comput Methods Appl Mech Eng 200(9–12):1220–1236
50. Nguyen VP, Lloberas-Valls O, Stroeven M, Sluys LJ (2012) Computational homogenization for multiscale crack modeling. Implementational and computational aspects. Int J Numer Methods Eng 89:192–226
51. Nguyen-Xuan H, Hoang T, Nguyen VP (2014) An isogeometric analysis for elliptic homogenization problems. Comput Methods Appl Mech Eng 67(9):1722–1741
52. Svenning E, Fagerström M, Larsson F (2016) On computational homogenization of microscale crack propagation. Int J Numer Meth Eng 108:76–90
53. Zhang R, Zhang L, Wang R, Zhao Y, Huang R (2016) Simulation of a multistage fractured horizontal well with finite conductivity in composite shale gas reservoir through finite-element method. ACS Energy Fuels 30:9036–9049
54. Tene M, Kobaisi MSA, Hajibeygi H (2016) Algebraic multiscale method for flow in heterogeneous porous media with embedded discrete fractures (F-AMS). J Comput Phys 321:819–845
55. Sheng Y, Sousani M, Ingham D, Pourkashanian M (2015) Recent developments in multiscale and multiphase modelling of the hydraulic fracturing process. Math Probl Eng 2015:729672
56. Liu Y, Filonova V, Hu N, Yuan Z, Fish J, Yuan Z, Belytschko T (2014) A regularized phenomenological multiscale damage model. Int J Numer Methods Eng 99:867–887
57. Paggi M, Wriggers P (2011) A nonlocal cohesive zone model for finite thickness interfaces—Part I: mathematical formulation and validation with molecular dynamics. Comput Mater Sci 50:1625–1633
58. Paggi M, Wriggers P (2011) A nonlocal cohesive zone model for finite thickness interfaces—Part II: FE implementation and application to polycrystalline materials. Comput Mater Sci 50(5):1634–1643
59. Paggi M, Reinoso J (2015) An anisotropic large displacement cohesive zone model for fibrillar and crazing of interfaces. Int J Solids Struct 69–70:106–120
60. Shojaei A, Li G, Fish J, Tan PJ (2014) Multi-scale constitutive modeling of ceramic matrix composites by continuum damage mechanics. Int J Solids Struct 51:4068–4081
61. Greco F, Leonetti L, Luciano R, Blasi PN (2016) An adaptive multiscale strategy for the damage analysis of masonry modeled as a composite material. Compos Struct 153:972–988
62. Nemat-Nasser S, Hori M (1993) Micromechanics: overall properties of heterogeneous materials. Elsevier, Amsterdam
63. Verhoosel CV, Remmers JJC, Gutiérrez MA (2010) A partition of unity-based multiscale approach for modelling fracture in piezoelectric ceramics. Int J Numer Methods Eng 82:966–994
64. Oliver J, Caicedo M, Huespe AE, Hernández JA, Roubin E (2017) Reduced order modeling strategies for computational multiscale fracture. Comput Methods Appl Mech Eng 313:560–595
65. Xu M, Gracie R, Belytschko T (2009) Bridging the Scales in Science and Engineering. In: Fish J (ed) Multiscale modeling with extended bridging domain method. Oxford University Press, Oxford
66. Rabczuk T (2013) Computational methods for fracture in brittle and quasi-brittle solids: state-of-the-art review and future perspectives. Appl Math 2013:849231
67. Ghayour M, Hosseini-Toudeshky H, Jalalvand M, Barbero EJ (2016) Micro/macro approach for prediction of matrix cracking evolution in laminated composites. J Compos Mater 50(19):2647–2659
68. Kerfriden P, Passieux JC, Bordas SPA (2012) Local/global model order reduction strategy for the simulation of quasi-brittle fracture. Int J Numer Methods Eng 89:154–179
69. Ojo SO, Budarapu PR, Paggi M (2017) A nonlocal adaptive discrete empirical interpolation method combined with modified hp-refinement for order reduction of molecular dynamics systems. Comput Mater Sci 140:189–208

70. Budarapu PR, Reinoso J, Paggi M (2017) Concurrently coupled solid shell-based adaptive multiscale method for fracture. Comput Methods Appl Mech Eng 319:338–365. doi:10.1016/j.cma.2017.02.023
71. Bischoff M, Ramm E (1997) Shear deformable shell elements for large strains and rotations. Int J Numer Methods Eng 40:4427–4449
72. Miehe C (1998) A theoretical and computational model for isotropic elastoplastic stress analysis in shells at large strains. Comput Methods Appl Mech Eng 155:193–233
73. Reinoso J, Paggi M (2014) A consistent interface element formulation for geometrical and material nonlinearities. Comput Mech 54(6):1569–1581
74. Reinoso J, Blázquez A (2016) Application and finite element implementation of 7-parameter shell element for geometrically nonlinear analysis of layered CFRP composites. Compos Struct 139:263–273
75. Reinoso J, Paggi M, Areias PMA (2016) A finite element framework for the interplay between delamination and buckling of rubber-like bi-material systems and stretchable electronics. J Eur Ceram Soc 36(9):2371–2382
76. Plimpton S (1995) Fast parallel algorithms for short-range molecular dynamics. J Comput Phys 117:1–19
77. Sproul A (2003) Solar cells resources for the secondary science teacher, chapter understanding the p-n junction. University of New South Wales, Sydney
78. Köntges M, Kunze I, Kajari-Schröder S, Breitenmoser X, Bjrneklett B (2011) The risk of power loss in crystalline silicon based photovoltaic modules due to microcracks. Sol Energy Mater Sol Cells 95:1131–1137
79. Paggi M, Sapora A (2013) Numerical modelling of microcracking in PV modules induced by thermo-mechanical loads. Energy Proc 38:506–515
80. Paggi M, Berardone I, Infuso A, Corrado M (2014) Fatigue degradation and electric recovery in Silicon solar cells embedded in photovoltaic modules. Sci Rep 4:4506
81. Käsewieter J, Haase F, Larrodé MH, Köntges M (2014) Cracks in solar cell metallization leading to module power loss under mechanical loads. Energy Proc 27:469–477
82. Yang H, Wang H, Cao D, Sun D, Ju X (2015) Analysis of power loss for crystalline silicon solar module during the course of encapsulation. Int J Photoenergy 2015:251615
83. Paggi M, Kajari-Schröder S, Eitner U (2011) Thermo-mechanical deformations in photovoltaic laminates. J Strain Anal Eng Des 46(8):772–782
84. Infuso A, Corrado M, Paggi M (2014) Image analysis of polycrystalline solar cells and modelling of intergranular and transgranular cracking. J Eur Ceram Soc 34(11):2713–2722
85. Paggi M, Corrado M, Berardone I (2016) A global/local approach for the prediction of the electric response of cracked solar cells in photovoltaic modules under the action of mechanical loads. Eng Fract Mech 168:40–57
86. Liang T, Shan T-R, Cheng Y-T, Devine BD, Noordhoek M, Li Y, Lu Z, Phillpot SR, Sinnott SB (2013) Classical atomistic simulations of surfaces and heterogeneous interfaces with the charge-optimized many body (COMB) potentials. Mater Sci Eng R 74:255–279
87. Ramisetti SB, Anciaux G, Molinari JF (2013) Spatial filters for bridging molecular dynamics with finite elements at finite temperatures. Comput Methods Appl Mech Eng 253:28–38
88. Mulay SS, Becker G, Vayrette R, Raskin JP, Pardoen T, Galceran M, Godet S, Noels L (2015) Multiscale modelling framework for the fracture of thin brittle polycrystalline films: application to polysilicon. Comput Mech 55:73–91
89. Verlet L (1967) Computer "experiments" on classical fluids. I. Thermodynamical properties of Lennard–Jones molecules. Phys Rev 159(5):98–103
90. Abraham FF, Broughton JQ, Bernstein N, Kaxiras E (1998) Spanning the length scales in dynamic simulation. Comput Phys 12:538–546
91. Novoselov KS, Geim AK, Morozov SV, Jiang D, Katsnelson MI, Grigorieva IV, Dubonos SV, Firsov AA (2005) Two-dimensional gas of massless Dirac fermions in graphene. Nature 438:197–200
92. Khare R, Mielke SL, Paci JT, Zhang S, Ballarini R, Schatz GC, Belytschko T (2007) Coupled quantum mechanical/molecular mechanical modeling of the fracture of defective carbon nanotubes and graphene sheets. Phys Rev B 75:075412
93. Lu Q, Gao W, Huang R (2011) Atomistic simulation and continuum modeling of graphene nanoribbons under uniaxial tension. Modell Simul Mater Sci Eng 19:54006
94. Novoselov KS, Falko VI, Colombo L, Gellert PR, Schwab MG, Kim K (2012) A roadmap for graphene. Nature 490:192–400
95. Ansari R, Ajori S, Motevalli B (2012) Mechanical properties of defective single-layered graphene sheets via molecular dynamics simulation. Superlattices Microstruct 51:274–289
96. Xu M, Tabarraei A, Paci J, Oswald J, Belytschko T (2012) A coupled quantum/continuum mechanics study of graphene fracture. Int J Fract 173:163–173
97. Budarapu PR, Javvaji B, Sutrakar VK, Mahapatra DR, Zi G, Rabczuk T (2015) Crack propagation in graphene. J Appl Phys 118:064307
98. Budarapu PR, Javvaji B, Sutrakar VK, Mahapatra DR, Zi G, Paggi M, Rabczuk T (2017) Lattice orientation and crack size effect on the mechanical properties of graphene. Int J Fract 203(1):81–91. doi:10.1007/s10704-016-0115-9
99. Javvaji B, Budarapu PR, Sutrakar VK, Mahapatra DR, Zi G, Paggi M, Rabczuk T (2016) Mechanical properties of graphene: molecular dynamics simulations correlated to continuum based scaling laws. Comput Mater Sci 125:319–327

100. Amani J, Oterkus E, Areias P, Zi G, Nguyen-Thoi T, Rabczuk T (2016) A non-ordinary state-based peridynamics formulation for thermoplastic fracture. Int J Impact Eng 87:83–94
101. Wang HS (2015) A meshfree variational multiscale methods for thermo-mechanical material failure. Theoret Appl Fract Mech 75:1–7
102. Miehe C, Vallicotti D, Zäh DD (2015) Computational structural and material stability analysis in finite electro-elasto-statics of electro-active materials. Int J Numer Methods Eng 102:1605–1637
103. Thomas S, Ajith KM (2014) Molecular dynamics simulation of the thermo-mechanical properties of monolayer graphene sheet. Proc Mater Sci 5:489–498
104. Chih-Ping W, Kuan-Hao C, Ming-Wang Y (2008) A meshfree DRK-based collocation method for the coupled analysis of functionally graded magneto-electro-elastic shells and plates. Comput Model Eng Sci 35:181–214
105. Chih-Ping W, Jian-Sin W, Ming-Wang Y (2009) A DRK interpolation-based collocation method for the analysis of functionally graded piezoelectric hollow cylinders under electro-mechanical loads. Comput Model Eng Sci 52:1–37
106. Rodríguez GD, Tapia A, Siedel GD, Avilés F (2016) Influence of structural defects on the electrical properties of carbon nanotubes and their polymer composites. Adv Funct Mater. doi:10.1002/adem.201600116
107. Tiwary CS, Javvaji B, Kumar C, Mahapatra DR, Ozden S, Ajayan PM, Chattopadhyay K (2015) Chemical-free graphene by unzipping carbon nanotubes using cryo-milling. Carbon. doi:10.1016/j.carbon.2015.03.036
108. Tiwary CS, Vishnu D, Kole AK, Brahmanandam J, Mahapatra DR, Kumbhakar P, Chattopadhyay K (2015) Stabilization of the high-temperature and high-pressure cubic phase of ZnO by temperature-controlled milling. J Mater Sci. doi:10.1007/s10853-015-9394-1
109. Vu-Bac N, Lahmer T, Zhang Y, Zhuang X, Rabczuk T (2014) Stochastic predictions of interfacial characteristic of polymeric nanocomposites (PNCs). Compos B 59:80–95
110. Scott WRP, Hünenberger PH, Tironi IG, Mark AE, Billeter SR, Fennen J, Torda AE, Huber T, Krüger P, van Gunsteren WF (1999) The GROMOS biomolecular simulation package. J Phys Chem A 103:3596–3607
111. Schmid N, Christ CD, Christen M, Eichenberger AP, van Gunsteren WF (2012) Architecture, implementation and parallelisation of the GROMOS software for biomolecular simulation. Comput Phys Commun 183:890–903
112. Ferreira RJ, Ferreira MJU, dos Santos DJVA (2012) Insights on p-glycoprotein's efflux mechanism obtained by molecular dynamics simulations. J Chem Theory Comput 8(6):1853–1864
113. Abraham MJ, Murtola T, Schulz R, Páll S, Smith JC, Hess B, Lindahl E (2015) GROMACS: high performance molecular simulations through multi-level parallelism from laptops to supercomputers. SoftwareX 1–2:19–25
114. Barkaoui A, Tlili B, Vercher-Martínez A (2016) A multiscale modelling of bone ultrastructure elastic proprieties using finite elements simulation and neural network method. Comput Methods Programs Biomed 134:69–78
115. Harvey M, Giupponi G, De Fabritiis G (2009) ACEMD: accelerated molecular dynamics simulations in the microseconds timescale. J Chem Theory Comput 5:1632
116. Harvey M, De Fabritiis G (2009) An implementation of the smooth particle-mesh Ewald (PME) method on GPU hardware. J Chem Theory Comput 5:2371–2377
117. Agilemolecule (2016) http://www.biomolecular-modeling.com/abalone/. Stockholm University
118. Berendsen HJC, van der Spoel D, van Drunen R (1995) GROMACS: a message-passing parallel molecular dynamics implementation. Comput Phys Commun 91(1):43–56
119. Pearlman DA, Case DA, Caldwell JW, Ross WS, Cheatham TE, Bolt SD, Ferguson D, Seibel G, Kollman P (1995) AMBER, a package of computer programs for applying molecular mechanics, normal mode analysis, molecular dynamics and free energy calculations to simulate the structural and energetic properties of molecules. Comput Phys Commun 91(1):1–41
120. Martínez L, Andrade R, Birgin EG, Martínez JM (2009) PACKMOL: a package for building initial configurations for molecular dynamics simulations. J Comput Chem 30(13):2157–2164
121. Humphrey W, Dalke A, Schulten K (1996) VMD: visual molecular dynamics. J Mol Graph 14(1):33–38
122. Qian D, Wagner GJ, Liu WK (2003) A multiscale projection method for the analysis of carbon nanotubes. Comput Methods Appl Mech Eng 193(17–20):1603–1632
123. Qian D, Gondhalekar RH (2004) A virtual atom cluster approach to the mechanics of nanostructures. Int J Multiscale Comput Eng 2(2):277–289
124. Qian D, Chirputkar S (2014) Bridging scale simulation of lattice fracture using enriched space–time finite element method. Int J Numer Methods Eng 97:819–850
125. Huang T, Zhang YX, Yang C (2016) Multiscale modelling of multiple-cracking tensile fracture behaviour of engineered cementitious composites. Eng Fract Mech 160:52–66
126. Fereidoon A, Rajabpour M, Hemmatian H (2013) Fracture analysis of epoxy/SWCNT nanocomposite based on global–local finite element model. Compos B 54:400–408
127. Melenk JM, Babuska I (1996) The partition of unity finite element method: basic theory and applications. Comput Methods Appl Mech Eng 139(1–4):289–314

128. Cai Y, Zhuang X, Augarde C (2010) A new partition of unity finite element free from linear dependence problem and processing delta property. Comput Methods Appl Mech Eng 199:1036–1043
129. Rabczuk T, Belytschko T, Xiao SP (2004) Stable particle methods based on Lagrangian kernels. Comput Methods Appl Mech Eng 193(12–14):1035–1063
130. Belytschko T, Lu YY, Gu L (1994) Element-free galerkin methods. Int J Numer Methods Eng 37:229–256
131. Liu WK, Jun S, Zhang YF (1995) Reproducing kernel particle methods. Int J Numer Methods Fluids 20:1081–1106
132. Liu WK, Jun S, Li S, Adee J, Belytschko T (1995b) Reproducing kernel particle methods for structural dynamics. Int J Numer Methods Eng 38:1655–1679
133. Daux CC, Möes N, Dolbow J, Sukumar N, Belytschko T (2000) Arbitrary branched and intersecting cracks with the extended finite element method. Int J Numer Methods Eng 48:1741–1760
134. Sukumar N, Moës N, Moran B, Belytschko T (2000) Extended finite element method for three-dimensional crack modeling. Int J Numer Methods Eng 48:1549–1570
135. Zi G, Chen H, Xu JX, Belytschko T (2005) The extended finite element method for dynamic fractures. Shock Vib 12(1):9–23
136. Areias PMA, Belytschko T (2005) Non-linear analysis of shells with arbitrary evolving cracks using XFEM. Int J Numer Methods Eng 62:384–415
137. Areias PMA, Belytschko T (2005) Analysis of three-dimensional crack initiation and propagation using the extended finite element method. Int J Numer Methods Eng 63:760–788
138. Bordas SPA, Rabczuk T, Nguyen-Xuan H, Natarajan S, Bog T, Nguyen VP, Do MQ, Nguyen VH (2010) Strain smoothing in FEM and XFEM. Comput Struct 88(23–24):1419–1443
139. Bordas SPA, Natarajan S, Pont SD, Rabczuk T, Kerfriden P, Mahapatra DR, Noel D, Gao Z, Gao Z (2011) On the performance of strain smoothing for enriched finite element approximations (XFEM/GFEM/PUFEM). Int J Numer Methods Eng 86(4–5):637–666
140. Nanthakumar SS, Lahmer T, Rabczuk T (2013) Detection of flaws in piezoelectric structures using xfem. Int J Numer Methods Eng 96(6):373–389
141. Nanthakumar SS, Lahmer T, Rabczuk T (2014) Detection of multiple flaws in piezoelectric structures using XFEM and level sets. Comput Methods Appl Mech Eng 275:98112
142. Nguyen-Thanh N, Kiendl J, Nguyen-Xuan H, Wuchner R, Bletzinger KU, Bazilevs Y, Rabczuk T (2011) Rotation free isogeometric thin shell analysis using PHT-splines. Comput Methods Appl Mech Eng 200(47–48):3410–3424
143. Nguyen-Xuan H, Liu GR, Bordas SPA, Natarajan S, Rabczuk T (2013) An adaptive singular ES-FEM for mechanics problems with singular field of arbitrary order. Comput Methods Appl Mech Eng 253:252–273
144. Vu-Bac N, Nguyen-Xuan H, Chen L, Bordas SPA, Kerfriden P, Simpson RN, Liu GR, Rabczuk T (2011) A noded-based smoothed XFEM for fracture mechanics. Comput Model Eng Sci 73:331–356
145. Strouboulis T, Copps K, Babuska I (2000) The generalized finite element method: an example of its implementation and illustration of its performance. Int J Numer Methods Eng 47:1401–1417
146. Strouboulis T, Copps K, Babuska I (2001) The generalized finite element method. Comput Methods Appl Mech Eng 190(32–33):4081–4193
147. Strouboulis T, Zhang L, Babuska I (2003) Generalized finite element method using mesh-based handbooks: application to problems in domains with many voids. Comput Methods Appl Mech Eng 192(28):3109–3161
148. Strouboulis T, Babuska I, Hidajat R (2006) The generalized finite element method for Helmholtz equation: theory, computation, and open problems. Comput Methods Appl Mech Eng 195:4711–4731
149. Strouboulis T, Hidajat R, Babuska I (2008) The generalized finite element method for helmholtz equation, Part II: effect of choice of handbook functions, error due to absorbing boundary conditions and its assessment. Comput Methods Appl Mech Eng 197:364–380
150. Babuska I, Banerjee U, Osborn JE (2004) Generalized finite element methods: main ideas, results, and perspective. Int J Comput Methods 1(1):67–103
151. Rabczuk T, Zi G (2007a) A meshfree method based on the local partition of unity for cohesive cracks. Comput Mech 39:743–760
152. Rabczuk T, Bordas SP, Zi G (2007b) A three-dimensional meshfree method for continuous multiple-crack initiation, propagation and junction in statics and dynamics. Comput Mech 40(3):473–495
153. Zi G, Rabczuk T, Wall W (2007) Extended meshfree methods without branch enrichment for cohesive cracks. Comput Mech 40(2):367–382
154. Bordas SPA, Rabczuk T, Zi G (2008) Three-dimensional crack initiation, propagation, branching and junction in non-linear materials by an extended meshfree method without asymptotic enrichment. Eng Fract Mech 75(5):943–960
155. Rabczuk T, Zi G, Bordas S, Nguyen-Xuan H (2008) A geometrically non-linear three dimensional cohesive crack method for reinforced concrete structures. Eng Fract Mech 75(16):4740–4758
156. Rabczuk T, Samaniego E (2008) Discontinuous modelling of shear bands using adaptive meshfree methods. Comput Methods Appl Mech Eng 197(6–8):641–658
157. Rabczuk T, Gracie R, Song J-H, Belytschko T (2010) Immersed particle method for fluid-structure interaction. Int J Numer Methods Eng 81(1):48–71
158. Ventura G, Xu XJ, Belytschko T (2002) A vector level set method and new discontinuity approximations

for crack growth by EFG. Int J Numer Methods Eng 54:923–944
159. Rabczuk T, Belytschko T (2004) Cracking particles: a simplified meshfree method for arbitrary evolving cracks. Int J Numer Methods Eng 61:2316–2343
160. Rabczuk T, Areias PMA (2006) A new approach for modelling slip lines in geological materials with cohesive models. Int J Numer Anal Methods Eng 30(11):1159–1172
161. Rabczuk T, Belytschko T (2006) Application of particle methods to static fracture of reinforced concrete structures. Int J Fract 137(1–4):19–49
162. Rabczuk T, Belytschko T (2007) A three dimensional large deformation meshfree method for arbitrary evolving cracks. Comput Methods Appl Mech Eng 1960(29–30):2777–2799
163. Rabczuk T, Areias PMA, Belytschko T (2007) A meshfree thin shell method for nonlinear dynamic fracture. Int J Numer Methods Eng 72(5):524–548
164. Rabczuk T, Song JH, Belytschko T (2009) Simulations of instability in dynamic fracture by the cracking particles method. Eng Fract Mech 76(6):730–741
165. Rabczuk T, Zi G, Bordas SP, Nguyen-Xuan H (2010) A simple and robust three-dimensional cracking-particle method without enrichment. Comput Methods Appl Mech Eng 199(37–40):2437–2455
166. Vu-Bac N, Nguyen-Xuan H, Chen L, Bordas SPA, Zhuang X, Liu GR, Rabczuk T (2013) A phantom-node method with edge-based strain smoothing for linear elastic fracture mechanics. J Appl Math. doi:10.1155/2013/978026
167. Chau-Dinh T, Zi G, Lee PS, Song JH, Rabczuk T (2010) Phantom-node method for shell models with arbitrary cracks. Comput Struct 92–93:242–256
168. Rabczuk T, Zi G, Gerstenberger A, Wall WA (2008) A new crack tip element for the phantom node method with arbitrary cohesive cracks. Int J Numer Methods Eng 75(5):577–599
169. Song JH, Areias PMA, Belytschko T (2006) A method for dynamic crack and shear band propagation with phantom nodes. Int J Numer Methods Eng 67(6):868–893
170. Hansbo A, Hansbo P (2004) A finite element method for the simulation of strong and weak discontinuities in solid mechanics. Comput Methods Appl Mech Eng 193(33–35):3523–3540
171. Mergheim J, Kuhl E, Steinmann P (2005) A finite element method for the computational modelling of cohesive cracks. Int J Numer Methods Eng 63:276–289
172. Mergheim J, Kuhl E, Steinmann P (2007) Towards the algorithmic treatment of 3d strong discontinuities. Commun Numer Methods Eng 23:97–108
173. Cai Y, Zhuang X, Zhu H (2013) A generalized and efficient method for finite cover generation in the numerical manifold method. Int J Comput Methods 10(5):1350028
174. Guowei M, Xinmei A, Lei H (2010) The numerical manifold method: a review. Int J Comput Methods 7(1):1–32
175. Miehe C, Welschinger F, Hofacker M (2010) Thermodynamically consistent phase-field models of fracture: variational principles and multi-field FE implementations. Int J Numer Methods Eng 83(10):1273–1311
176. Miehe C, Hofacker M, Welschinger F (2010) A phase field model for rate-independent crack propagation: robust algorithmic implementation based on operator splits. Comput Methods Appl Mech Eng 199:2765–2778
177. Msekh MA, Sargado M, Jamshidian M, Areias P, Rabczuk T (2015) ABAQUS implementation of phase-field model for brittle fracture. Comput Mater Sci 96B:472–484
178. Amiri F, Millán D, Shen Y, Rabczuk T, Arroyo M (2014) Phase-field modeling of fracture in linear thin shells. Theoret Appl Fract Mech 69:102–109
179. Seleson P, Beneddine S, Prudhomme S (2013) A force-based coupling scheme for peridynamics and classical elasticity. Comput Mater Sci 66:34–49
180. Tong Q, Li S (2016) Multiscale coupling of molecular dynamics and peridynamics. J Mech Phys Solids 95:169–187
181. Hughes TJR, Cottrell J, Bazilevs Y (2005) Isogeometric analysis: CAD, finite elements, NURBS, exact geometry and mesh refinement. Comput Methods Appl Mech Eng 194:4135–4195
182. Bazilevs Y, Calo VM, Cottrell JA, Evans JA, Hughes TJR, Lipton S, Scott MA, Sederberg TW (2010) Isogeometric analysis using T-splines. Comput Methods Appl Mech Eng 199(5–8):229–263
183. Nguyen VP, Nguyen-Xuan H (2013) High-order b-splines based finite elements for the delamination analysis of laminated composites. Compos Struct 102:261–275
184. Chien HT, Ferreira AJ, Carrera E, Nguyen-Xuan H (2013) Isogeometric analysis of laminated composite and sandwich plates using a layerwise deformation theory. Compos Struct 104:196–214
185. Chien HT, Ferreira AJM, Rabczuk T, Bordas SPA, Nguyen-Xuan H (2014) Isogeometric analysis of laminated composite and sandwich plates using a new inverse trigonometric shear deformation theory. Eur J Mech A Solids 43:89–108
186. Nguyen-Xuan H, Thai CH, Nguyen-Thoi T (2013) Isogeometric finite element analysis of composite sandwich plates using a new higher order shear deformation theory. Compos Part B 55:558–574
187. Areias PMA, Rabczuk T (2013) Finite strain fracture of plates and shells with configurational forces and edge rotations. Int J Numer Methods Eng 94:1099–1122
188. Rabczuk T, Areias PMA (2006) A meshfree thin shell for arbitrary evolving cracks based on an extrinsic basis. Comput Model Eng Sci 16(2):115–130

189. Nguyen-Thanh N, Valizadeh N, Nguyen MN, Nguyen-Xuan H, Zhuang X, Areias P, Zi G, Bazilevs Y, De Lorenzis L, Rabczuk T (2015) An extended isogeometric thin shell analysis based on Kirchhoff–Love theory. Comput Methods Appl Mech Eng 284:265–291
190. Plews JA, Duarte CA (2016) A two-scale generalized finite element approach for modeling localized thermoplasticity. Int J Numer Methods Eng 108:1123–1158
191. Akkutlu IY, Efendiev Y, Vasilyeva M (2016) Multiscale model reduction for shale gas transport in fractured media. Comput Geosci 20:953–973
192. Efendiev E (2015) Generalized multiscale finite element methods (GMsFEM). J Comput Phys 251:116–135
193. Belytschko T, Black T (1999) Elastic crack growth in finite elements with minimal remeshing. Int J Numer Methods Eng 45(5):601–620
194. Moës N, Dolbow J, Belytschko T (1999) A finite element method for crack growth without remeshing. Int J Numer Methods Eng 46(1):131–150
195. Belytschko T, Gracie R, Ventura G (2009) A review of extended/generalized finite element methods for material modeling. Model Simul Mater Sci Eng 17:043001
196. Fries T-P, Belytschko T (2010) The extended/generalized finite element method: an overview of the method and its applications. Int J Numer Methods Eng 84(3):253–304
197. Karihaloo BL, Xiao QZ (2003) Modelling of stationary and growing cracks in fe framework without remeshing: a state-of the-art review. Comput Struct 81(3):119–129
198. Mohammadi S (2008) Extended finite element method for fracture analysis of structures, vol Oxford. Blackwell Publishing, Hoboken
199. Nguyen VP, Rabczuk T, Bordas SP, Duflot M (2008) Meshless methods: a review and computer implementation aspects. Math Comput Simul 79(3):763–813
200. Belytschko T, Tabbara M (1996) Dynamic fracture using element-free Galerkin methods. Int J Numer Methods Eng 39:923–938
201. Bauman P, Dhia H, Elkhodja N, Oden J, Prudhomme S (2008) On the application of the Arlequin method to the coupling of particle and continuum models. Comput Mech 42(4):511–530
202. Amiri F, Anitescu C, Arroyo M, Bordas S, Rabczuk T (2014) XLME interpolants, a seamless bridge between xfem and enriched meshless methods. Comput Mech 53(1):45–57
203. Atluri SN, Shengping S (2002) The meshless local Petrov-Galerkin (MLPG) method: a simple and less-costly alternative to the finite element and boundary element methods. Comput Model Eng Sci 3(1):11–51
204. Liu K, Long S, Li G (2006) A simple and less-costly meshless local Petrov-Galerkin (MLPG) method for the dynamic fracture problem. Eng Anal Boundary Elem 30(1):72–76
205. Liu GR, Gu YT (2001) A local radial point interpolation method (LRPIM) for free vibration analyses of 2-D solids. J Sound Vib 246(1):29–46
206. Liu GR, Zhang GY, Gu YT, Wang YY (2005) A meshfree radial point interpolation method (RPIM) for three-dimensional solids. Comput Mech 36(6):421–430
207. Shih-Wei Y, Yung-Ming W, Chih-Ping W, Hsuan-Teh H (2010) A meshless collocation method based on the differential reproducing kernel approximation. Comput Model Eng Sci 60:1–39
208. Zhuang X, Augarde C, Mathisen K (2012) Fracture modelling using meshless methods and level sets in 3D: framework and modelling. Int J Numer Methods Eng 92:969–998
209. Chih-Ping W, Shih-Wei Y, Ming-Wang Y, Hsuan-Teh H (2011) A meshless collocation method for the plane problems of functionally graded material beams and plates using the DRK interpolation. Mech Res Commun 38:471–476
210. Yung-Ming W, Syuan-Mu C, Chih-Ping W (2010) A meshless collocation method based on the differential reproducing kernel interpolation. Comput Mech 45:585–606
211. Griffith AA (1921) The phenomena of rapture and flow in solids. Philos Trans R Soc Lond A 221:163–198
212. Irwin G (1957) Analysis of stresses and strains near the end of a crack traversing a plate. J Appl Mech 24:361–364
213. Kuhn C, Müller R (2010) A continuum phase field model for fracture. Eng Fract Mech 77(18):3625–3634
214. Karma A, Kessler DA, Levine H (2001) Phase-field model of mode III dynamic fracture. Phys Rev Lett 87:045501
215. Borden MJ, Hughes TJR, Landis CM, Verhoosel CV (2014) A higher-order phase-field model for brittle fracture. Comput Methods Appl Mech Eng 273:100–118
216. Areias P, Rabczuk T, Msekh MA (2016) Phase-field analysis of finite-strain plates and shells including element subdivision. Comput Methods Appl Mech Eng 312:322–350
217. Yingjun G, Zhirong L, Lilin H, Hong M (2016) Phase field crystal study of nano-crack growth and branch in materials. Modell Simul Mater Sci Eng 24:055010
218. Giovanardi B, Scotti A, Formaggia L (2017) A hybrid XFEM-phase field (Xfield) method for crack propagation in brittle elastic materials. Comput Methods Appl Mech Eng. doi:10.1016/j.cma.2017.03.039
219. Areias PMA, Song JH, Belytschko T (2006) Analysis of fracture in thin shells by overlapping paired elements. Comput Methods Appl Mech Eng 195:5343–5360
220. Liu WK, Qian D, Gonella S, Li S, Chen W, Chirputkar S (2010) Multiscale methods for mechanical science of complex materials: bridging from quantum to stochastic multiresolution continuum. Int J Numer Methods Eng 83:1039–1080

221. Chen H, Zang M, Zhang YX (2016) A ghost particle-based coupling approach for the combined finite-discrete element method. Finite Elem Anal Des 114:68–77
222. Kojic M, Filipovic N, Tsuda A (2008) A mesoscopic bridging scale method for fluids and coupling dissipative particle dynamics with continuum finite element method. Comput Methods Appl Mech Eng 197(6–8):821–833
223. Li X, Wan K (2011) A bridging scale method for granular materials with discrete particle assembly-cosserat continuum modeling. Comput Geotech 38:1052–1068
224. Kadowaki H, Liu WK (2004) Bridging multi-scale method for localization problems. Comput Methods Appl Mech Eng 193(30–32):3267–3302
225. Tang S, Hou TY, Liu WK (2006) A mathematical framework of the bridging scale method. Int J Numer Methods Eng 65:1688–1713
226. Wang W, Chang K-H (2013) Continuum-based sensitivity analysis for coupled atomistic and continuum simulations for 2-d applications using bridging scale decomposition. Struct Multidiscipl Optim 47:867–892
227. Guidault PA, Belytschko T (2007) On the L^2 and the H^1 couplings for an overlapping domain decomposition method using lagrange multipliers. Int J Numer Methods Eng 70:322–350
228. Gracie R, Belytschko T (2011) Adaptive continuum-atomistic simulations of dislocation dynamics. Int J Numer Methods Eng 86(4–5):575–597
229. Belytschko T, Xiao SP (2004) A bridging domain method for coupling continua with molecular dynamics. Comput Methods Appl Mech Eng 193(17–20):1645–1669
230. Fish J, Chen W (2004) Discrete-to-continuum bridging based on multigrid principles. Comput Methods Appl Mech Eng 193:1693–1711
231. Tabarraei A, Wang X, Sadeghirad A, Song JH (2014) An enhanced bridging domain method for linking atomistic and continuum domains. Finite Elem Anal Des 92:36–49
232. Xu M, Belytschko T (2008) Conservation properties of the bridging domain method for coupled molecular/continuum dynamics. Int J Numer Methods Eng 76:278–294
233. Xu M, Gracie R, Belytschko T (2010) A continuum-to-atomistic bridging domain method for composite lattices. Int J Numer Methods Eng 81:1635–1658
234. Anciaux G, Ramisetti SB, Molinari JF (2012) A finite temperature bridging domain method for MD-FE coupling and application to a contact problem. Comput Methods Appl Mech Eng 205–208:204–212
235. Tu F, Ling D, Bu L, Yang Q (2014) Generalized bridging domain method for coupling finite elements with discrete elements. Comput Methods Appl Mech Eng 276:509–533
236. Gurtin ME, Podio-Guidugli P (1996) Configurational forces and the basic laws for crack propagation. J Mech Phys Solids 44(6):905–927
237. Gurtin ME, Podio-Guidugli P (1998) Configurational forces and a constitutive theory for crack propagation that allows for kinking and curving. J Mech Phys Solids 46(8):1343–1378
238. Miehe C, Gürses E (2007) A robust algorithm for configurational-force-driven brittle crack propagation with radaptive mesh alignment. Int J Numer Methods Eng 72(2):127–157
239. Mosler J (2009) A variationally consistent approach for crack propagation based on configurational forces. In: IUTAM symposium on progress in the theory and numerics of configurational mechanics, vol 17. IUTAM Bookseries, pp 239–247
240. Sih GC (1974) Strain-energy-density factor applied to mixed mode crack problems. Int J Fract 10(3):305–321
241. Wu CH (1978) Fracture under combined loads by maximum energy release rate criterion. J Appl Mech Trans ASME 45(3):553–558
242. Goldstein RV, Salganik RL (1974) Brittle fracture of solids with arbitrary cracks. Int J Fract 10(4):507–523
243. Benedetti I, Aliabadi MH (2015) Multiscale modeling of polycrystalline materials: a boundary element approach to material degradation and fracture. Comput Methods Appl Mech Eng 289:429–453
244. Cynthia LK, Plimpton SJ, Hamilton JC (1998) Dislocation nucleation and defect structure during surface indentation. Phys Rev B 58:11085
245. Budarapu PR, Gracie R, Yang S-W, Zhuang X, Rabczuk T (2014) Efficient coarse graining in multiscale modeling of fracture. Theoret Appl Fract Mech 69:126–143
246. Dipasquale D, Zaccariotto M, Galvanetto U (2014) Crack propagation with adaptive grid refinement in 2D peridynamics. Int J Fract 190:1–22
247. Unger JF (2013) An fe^2-x^1 approach for multiscale localization phenomena. J Mech Phys Solids 61:928–948
248. Park K, Paulino GH, Celes W, Espinha R (2012) Adaptive mesh refinement and coarsening for cohesive zone modeling of dynamic fracture. Int J Numer Methods Eng 92:1–35
249. Belytschko T, Song JH (2010) Coarse-graining of multiscale crack propagation. Int J Numer Methods Eng 81(5):537–563
250. Miller RE, Tadmor EB (2009) A unified framework and performance benchmark of fourteen multiscale atomistic/continuum coupling methods. Model Simul Mater Sci Eng 17:053001
251. Nair AK, Warner DH, Hennig RG (2011) Coupled quantum-continuum analysis of crack tip processes in aluminum. J Mech Phys Solids 59(12):2476–2487
252. Liu W, Hong J-W (2012) A coupling approach of discretized peridynamics with finite element method. Comput Methods Appl Mech Eng 245–246:163–175

253. Talebian M, Al-Khoury R, Sluys LJ (2013) A computational model for coupled multiphysics processes of CO_2 sequestration in fractured porous media. Adv Water Resour 59:238–255
254. Jothi S, Croft TN, Brown SGR (2015) Multiscale multiphysics model for hydrogen embrittlement in polycrystalline nickel. J Alloys Compd 645:S500–S504
255. Reifsnider K, Raihan MDR, Vadlamudi V (2016) Heterogeneous fracture mechanics for multi-defect analysis. Compos Struct 156:20–28
256. Grujicic M, Ramaswami S, Yavari R, Galgalikar R (2016) Multiphysics computational analysis of white-etch cracking failure mode in wind turbine gearbox bearings. Proc IMechE Part L J Mater Des Appl 230(1):43–63
257. Wu W, Xiao X, Huang X, Yan S (2014) A multiphysics model for the in situ stress analysis of the separator in a lithium-ion battery cell. Comput Mater Sci 83:127–136
258. Jiang T, Rudraraju S, Roy A, Van der Ven A, Garikipati K, Falk ML (2016) Multiphysics simulations of lithiation-induced stress in Li_{1+x} Ti_2O_4 electrode particles. J Phys Chem C 120:27871–27881
259. PantanoMF Bernai RA, Pagnotta L, Espinosa HD (2015) Multiphysics design and implementation of a microsystem for displacement-controlled tensile testing of nanomaterials. Meccanica 50:549–569
260. Saft A, Kaliske M (2013) A hybrid interface-element for the simulation of moisture-induced cracks in wood. Eng Fract Mech 102:32–50
261. Yu M-F, Lourie O, Dyer MJ, Moloni K, Kelly TF, Ruoff RS (2000) Strength and breaking mechanism of multiwalled carbon nanotubes under tensile load. Science 287:637–640
262. Mielke SL, Troya D, Zhang S, Li J-L, Xiao S, Car R, Ruoff RS, Schatz GC, Belytschko T (2004) The role of vacancy defects and holes in the fracture of carbon nanotubes. Chem Phys Lett 390:413–420
263. Svensson MM, Humbel S, Froese RDJ, Matsubara T, Sieber S, Morokuma K (1996) ONIOM: a multilayered integrated MO + MM method for geometry optimizations and single point energy predictions. A test for Diels Alder reactions and Pt(P(t-Bu)3)2+H2 oxidative addition. J Phys Chem 100:19357–19363
264. Khare R, Mielke SL, Schatz GC, Belytschko T (2008) Multiscale coupling schemes spanning the quantum mechanical, atomistic forcefield, and continuum regimes. Comput Methods Appl Mech Eng 197:3190–3202
265. Park JY, Park CH, Park JS, Kong K-J, Chang H, Im S (2010) Multiscale computations for carbon nanotubes based on a hybrid QM/QC (quantum mechanical and quasicontinuum) approach. J Mech Phys Solids 58:86–102
266. Silling SA (2000) Reformulation of elasticity theory for discontinuities and long-range forces. J Mech Phys Solids 48:175–209
267. Silling SA, Lehoucq RB (2010) Peridynamic theory of solid mechanics. Adv Appl Mech 44:73–166
268. Ren H, Zhuang X, Cai Y, Rabczuk T (2016) Dual-horizon peridynamics. Int J Numer Meth Eng 108(12):1451–1476
269. Ren H, Zhuang X, Rabczuk T (2017) Dual-horizon peridynamics: A stable solution to varying horizons. Comput Methods Appl Mech Eng 318:762–782
270. Parks ML, Lehoucq RB, Plimpton SJ, Silling SA (2008) Implementing peridynamics within a molecular dynamics code. Comput Phys Commun 179:777–783
271. Rahman R, Foster JT (2014) Bridging the length scales through nonlocal hierarchical multiscale modeling scheme. Comput Mater Sci 92:401–415
272. Brothers MD, Foster JT, Millwater HR (2014) A comparison of different methods for calculating tangent-stiffness matrices in a massively parallel computational peridynamics code. Comput Methods Appl Mech Eng 279:247–267
273. Zhang Y, Yao H, Ortiz C, Xu J, Dao M (2012) Bio-inspired interfacial strengthening strategy through geometrically interlocking designs. J Mech Behav Biomed Mater 15:70–77
274. Egan P, Sinko R, LeDuc PR, Keten S (2005) The role of mechanics in biological and bio-inspired systems. Nat Commun 6:7418
275. Tang Z, Kotov NA, Magonov S, Ozturk B (2003) Nanostructured artificial nacre. Nat Mater 2(6):413
276. Niebel TP, Bouville F, Kokkinis D, Studart AR (2016) Role of the polymer phase in the mechanics of nacre-like composites. J Mech Phys Solids 96:133–146
277. Awaja F, Zhang S, Tripathi M, Nikiforov A, Pugno N (2016) Cracks, microcracks and fracture in polymer structures: formation, detection, autonomic repair. Prog Mater Sci 83:536–573
278. Wang W, Elbanna A (2014) Crack propagation in bone on the scale of mineralized collagen fibrils: role of polymers with sacrificial bonds and hidden length. Bone 68:20–31
279. Fratzl P, Kolednik O, Fischer FD, Dean MN (2016) The mechanics of tessellations-bioinspired strategies for fracture resistance. Chem Soc Rev 45:252
280. Ma S, Scheider I, Bargmann S (2016) Continuum damage modeling and simulation of hierarchical dental enamel. Model Simul Mater Sci Eng 24:045014
281. Ural A, Mischinski S (2013) Multiscale modeling of bone fracture using cohesive finite elements. Eng Fract Mech 103:141–152
282. Rabiei R, Bekah S, Barthelat F (2010) Failure mode transition in nacre and bone-like materials. Acta Biomater 6:4081–4089

Dr. Budarapu is a faculty member in the School of Mechanical Sciences, Indian Institute of Technology, Bhubaneswar, India. Dr. Budarapu's research focus is mainly on computational methods for fracture and failure of solids. His primary interests are in developing adaptive multiscale methods and their application to materials and design for various applications. His areas of interests include: multiscale methods for fracture, molecular dynamics, fracture studies in multiphysics problems and polymer nano-composites.

T. Rabczuk is professor of computational mechanics at Institut für Strukturmechanik (ISM), Bauhaus Universität-Weimar, since 2009. The research focus of Prof. Rabczuk is Computational Solid Mechanics with emphasis on method development for problems involving fracture and failure of solids and fluid-structure interaction. He is particularly interested in developing multiscale methods and their application to computational materials design. His main research topics include: Constitutive Modeling, Material Instabilities, Fracture, Strain Localization, Numerical Methods (Extended Finite Element and Mesfhree Methods), Isogeometric Analysis, Computational Fluid-Structure Interaction and Biomechanical Engineering. He is the ISI Highly Cited Researcher (2014–2016) in the categories 'Computer Science' and 'Engineering'.